The effect of reactor configuration on bioelectrochemical production of acetate from carbon dioxide

----

To mitigate global warming and its adverse effects, more sustainable alternatives for the fossil fuel-based production of energy and chemicals are needed. Acetogenic bacteria can reduce the greenhouse gas CO_2 into hydrocarbons like acetate using reducing equivalents supplied via a cathode in a bioelectrochemical system. However, the production process needs improvements to enable cost-effective production in an industrial scale.

To improve the process, a fluidized bed reactor (FluBR) was tested to enhance mass transfer. The tubular cathode chamber inside the cylindrical anode chamber hosted a mixed culture of acetogens and activated carbon granules, which were fluidized at a flow rate of 170 mL/min. As a control for fluidization, a fixed bed reactor (FixBR) was prepared by replacing the bed material with heavier graphite granules, while the flow rate was 250 mL/min.

Both reactors supported bioelectrochemical production of acetate reaching their peak performance 14 days after the acetate production had started. The maximum volumetric productivity was 0.21 g/L/d in the FluBR and 0.22 g/L/d in the FixBR while 37 % and 40 % of the electrons provided by the cathode were assimilated into acetate in the FluBR and the FixBR, respectively.

The performance of the FixBR and the FluBR were similar, but the differences between the reactor setups could have affected the results. The reactors need to be further tested for comparable results and optimized to improve the acetate production.

Keywords: Bioelectrochemical system, Biological fluidized bed, Mixed reactor microbiome, Acetogenesis

TURUN YLIOPISTO
Biokemian laitos
KARINSALO JANNIINA: Reaktorikonfiguraation vaikutus asetaatin biosähkökemialliseen tuottoon hiilidioksidista
Diplomityötutkielma, 49 s.
Biotekniikka
Elokuu 2020
Turun yliopiston laatujärjestelmän mukaisesti tämän julkaisun alkuperäisyys on tarkastettu Turnitin Originality Check -järjestelmällä

Ilmastonmuutoksen ja sen haittavaikutuksien vähentämiseksi tarvitaan kestävämpiä vaihtoehtoja fossiilisille polttoaineille ja kemikaaleille. Mikrobielektrosynteesissä asetogeeniset bakteerit käyttävät katodilta saatuja elektroneja hiilidioksidin pelkistämiseen muodostaen hiilivetyjä kuten asetaattia. Jotta menetelmää voitaisiin käyttää kustannustehokkaasti teollisessa mittakaavassa, tuottoprosessia pitäisi parantaa.

Työn tarkoitus oli parantaa mikrobielektrosynteesin tehokkuutta parantamalla massansiirtoa leijupetireaktorin avulla. Reaktorin sylinterimäisen anodikammion sisällä oli putkimainen katodikammio, jossa kasvatettiin asetogeeneja sisältävää sekaviljelmää. Katodikammioon lisättiin aktiivihiilirakeita, joita leijutettiin 170 ml/min virtausnopeudella. Leijupetireaktorin kontrollina käytettiin muuten samanlaista kiintopatjareaktoria, jossa aktiivihiilirakeiden sijaan käytettiin raskaampia grafiittirakeita, joiden läpi kasvatusmediumia kierrätettiin 250 ml/min virtausnopeudella.

Molemmat reaktorit tukivat asetaatin biosähkökemiallista muodostusta saavuttaen suurimmat tuottonsa ja tehokkuutensa 14 päivää asetaatin tuoton alkamisen jälkeen. Suurin volumetrinen tuottavuus oli 0.21 g/L/d leijupetireaktorissa ja 0.22 g/L/d kiintopatjareaktorissa. Lisäksi leijupetireaktorissa enimmillään 37 % ja kiintopatjareaktorissa enimmillään 40 % katodilta saaduista elektroneista hyödynnettiin asetaatin tuottoon.

Reaktorien tulokset olivat lähes samanlaiset, mutta reaktorien väliset erot esimerkiksi virtausnopeudessa ovat voineet vaikuttaa tuloksiin. Reaktoreita tulisi siis tutkia ja kehittää edelleen vertailukelpoisempien tulosten sekä parempien tehokkuuksien ja tuottavuuksien saavuttamiseksi.

Avainsanat: Mikrobielektrosynteesi, Biologinen leijupeti, Sekaviljelmä, Asetogeneesi

Table of contents

Abbreviations

abioFixBR	Abiotic fixed bed reactor
abioFluBR	Abiotic fluidized bed reactor
Acetyl-CoA	Acetyl coenzyme A
AEM	Anion exchange membrane
$A_{specific}$	Specific surface area
BES	Bioelectrochemical system
bioFixBR	Biotic fixed bed reactor
bioFluBR	Biotic fluidized bed reactor
CE	Coulombic efficiency
CEM	Cation exchange membrane
COD	Chemical oxygen demand
CV	Cyclic voltammetry
EET	Extracellular electron transfer
FixBR	Fixed bed reactor
FluBR	Fluidized bed reactor
GAC	Granular activated carbon
GDE	Gas diffusion electrode
GC	Gas chromatography
ID	Internal diameter
MEC	Microbial electrosynthesis cell
MES	Microbial electrosynthesis
MFC	Microbial fuel cell
p_{H2}	Hydrogen partial pressure
PEM	Proton exchange membrane
PPC	porous polymer carrier
OD_{600nm}	Optical density at 600 nm
SHE	Standard hydrogen electrode
SVR	Surface to volume ratio
VFA	Volatile fatty acid

1 Introduction

Fossil fuels have fulfilled the energy demand for the economic growth especially since the industrial revolution due to their advantages (Wringley 2013). They are energy-rich, available almost at all times and easily stored (Wrigley 2013), but in addition to being an energy source, they are suitable for other applications too. They can also be used in the chemical industry sector as feedstock to produce plastics and other hydrocarbons (Levi and Cullen 2018).

However, burning fossil resources release carbon, which increases the atmospheric CO_2 levels, which in turn raises the global temperature causing adverse environmental effects. Climate change can drive species to extinction, raise the sea level and increase the recurrence as well as the severity of storms, which may also affect human life. (Pandey 2002.) To alleviate the impacts of climate change, it is important to find renewable replacements for fossil fuels. Renewable energies such as solar energy have become accessible in the energy markets and have become available to the public, but their production is dependent on the weather or the sunny hours (Maric and Yu 2019). At the same time, nuclear power provides a more continuous electricity supply, but its environmental benefits are debated (Groh and Möllendorff 2020; Kim and Alameri 2019).

The advantage of electricity is its wide range of applications; it can light a bulb or fuel electric cars among other possibilities. Additionally, the excess electricity of intermittent renewable power could be stored to cover the non-productive phase (Maric and Yu 2019). On the other hand, the advantage of fossil fuel as a liquid fuel in the first place is the possibility to store it efficiently and use it on demand. Thus, a liquid fuel and chemical commodities from a renewable energy source, could have the advantages of a fossil fuel while providing a sustainable and environmentally friendly option (Marshall *et al.* 2012; Zhang and Angelidaki 2014).

However, the production of liquid fuels and chemicals from renewable energy sources by cultivating plant biomass on land is unsustainable, because the preparation of soil and the clearance of forests release carbon fixed in the biomass as well as in the soil. Production on agricultural land is not attractive unless the land has been left aside from food production. (Fargione *et al.* 2008.) On the same grounds, utilizing plant-based products (e.g. glucose) as substrates to produce chemicals such as ethanol could be conflicting.

The idea of converting atmospheric CO_2 into a product is appealing, and also some microorganisms are capable of turning CO_2 into value-added compounds and fuels without farmland (LaBelle *et al.* 2014). For the conversion of CO_2, the microorganisms need a power source, which could be the momentary excess electricity of renewable energy in an electrochemical cell (Marshall *et al.* 2012; Zhang and Angelidaki 2014).

1.1 Bioelectrochemical systems

Bioelectrochemical system (BES) is a combination of a bioreactor and an electrochemical cell, where the anode accepts electrons from oxidative reactions and the cathode donates electrons for reductive reactions (Krieg *et al.* 2018). In BES, microorganisms are introduced into the electrochemical system to function as the biocatalyst on the electrodes. Furthermore, the electrode catalysing the reactions of interest is the working electrode while the opposite electrode is the counter electrode. (Krieg *et al.* 2014.)

The mechanisms of the microbes to uptake or donate electrons extracellularly relies on extracellular electron transfer (EET), which can be direct or indirect depending on microbial capabilities and the involvement of electron carriers. In the case of indirect EET, the transfer is mediated by external electron carriers found in the environment or produced by some bacteria. The mechanisms of the direct EET are not fully understood, but biofilm plays an important role, in which conductive appendages in the cell membrane could mediate electrons between the cell and the electrode. (Kracke *et al.* 2015.)

Some anaerobic and usually acetogenic or methanogenic bacteria can potentially utilize an anode or/and a cathode for redox reactions. The reaction products depend greatly on the type of bacteria and the electrochemical mode of operation in addition to other factors. (Nevin *et al.* 2010; Zhang and Angelidaki 2014.)

1.1.1 Biotic anode applications

The biological treatment of wastewater requires energy. To make it more economical and efficient, different ways to produce energy or biofuels have been integrated into wastewater treatment. The biotic anode applications of BES could be used in wastewater treatment to generate electricity in a microbial fuel cell (MFC) or to produce biogas in a microbial electrolysis cell (MEC). (Haavisto *et al.* 2017; Zhang and Angelidaki 2014.)

According to Khanal (2008a) the redox reactions in MFC are similar to a hydrogen fuel cell, where H_2 is oxidized at the anode into electrons and protons, which are used at the

cathode to reduce O_2 into water as seen in Figure 1A (Khanal 2008a). Instead of H_2, organic matter is fed into the anodic chambers of MFC and MEC to be oxidized into CO_2 by anaerobic microbes, with concomitant release and transfer of electrons to the anode (Figure 1B & 1C). The transfer of electrons to the anode can be captured as electricity in MFC, whereas an additional power source is needed in MEC to make the formation of energy carrier like H_2 thermodynamically possible. (Logan *et al.* 2006; Rabaey and Rozendal 2010; Rozendal *et al.* 2006; Zhang and Angelidaki 2014.)
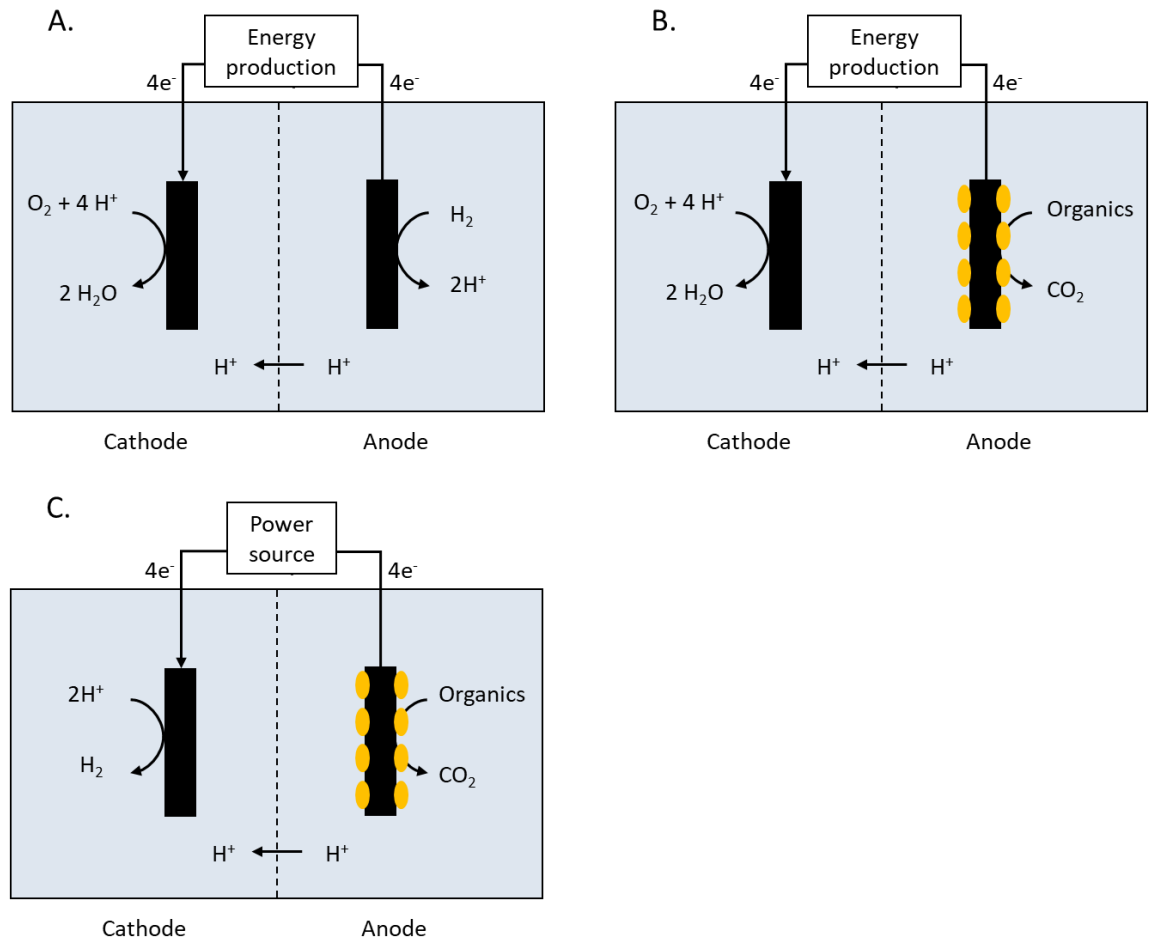
Figure 1. *(A) In a hydrogen fuel cell, oxidation of hydrogen at the anode and formation of water at the cathode generates electricity. (Adapted from Paul et al. 2019) (B) In microbial fuel cell, microbes oxidize organic compounds anaerobically at the anode, generating electricity. (Adapted from Vassilev 2019). (C) Additional power is needed in a microbial electrolysis cell to form e.g. hydrogen at the cathode anaerobically when anaerobic microbes oxidize organic matter at the anode (Adapted from Vassilev 2019).*

1.1.2 Microbial electrosynthesis – a biotic cathode

The redox reactions can also be triggered by applying electric potential if the reactions were otherwise be thermodynamically unfavourable in their ambient conditions such as the formation of H_2 under nearly neutral pH (Logan *et al.* 2019). One such example is an electrolytic cell, where an external current is applied to oxidize water into O_2 and protons

at the anode, and to reduce the protons into H_2 at the cathode (Figure 2A). A proton permeable membrane is used to separate the two chambers while enabling the diffusion of the protons from the anode to the cathode. (Maric and Yu 2019.) Additionally, microbial electrosynthesis (MES) converts electrical energy and CO_2 into chemical compounds using microorganisms as catalysts at the cathode (Figure 2B) (Blanchet *et al.* 2015).
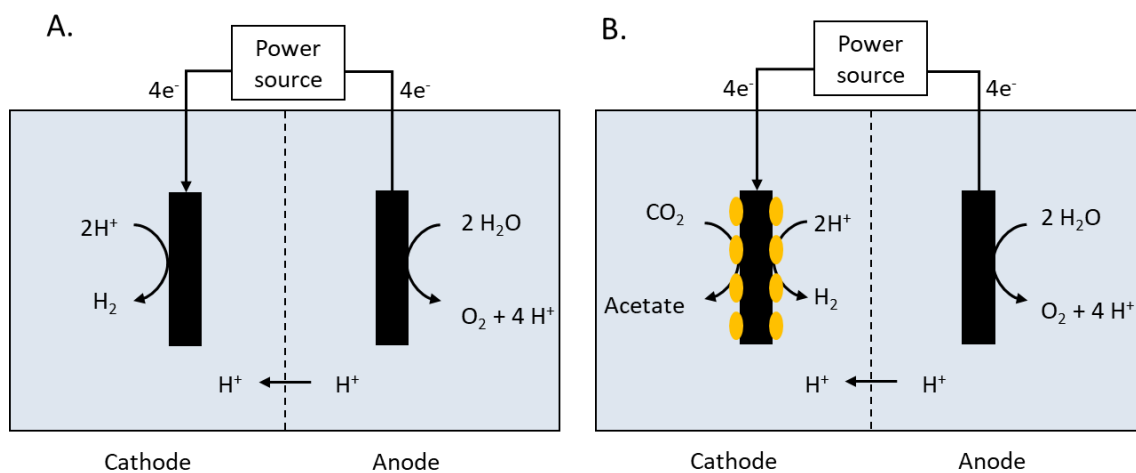
Figure 2. *(A) In the electrolysis of water, the water is oxidized at the anode and the released protons are then reduced into hydrogen at the cathode (Adapted from Maric and Yu 2019). (B) The same redox reactions happen in a microbial electrosynthesis (MES), but the anaerobic acetogens can utilize the hydrogen or electrons directly from the cathode to reduce CO_2 into acetate (Adapted from Vassilev 2019).*

The cathode in MES hosts autotrophic homoacetogens or hydrogenotrophic methanogens, both of which can reduce CO_2 (Molenaar *et al.* 2017). The homoacetogenic bacteria can reduce CO_2 into volatile fatty acids (VFA) such as acetate as seen in Figure 2B while the (hydrogenotrophic) methanogenic bacteria can reduce CO_2 into methane. In an anaerobic, syntrophic culture, the acetogens and the methanogens can acquire the reducing equivalents in form of H_2, produced by heterotrophic hydrogen-producing bacteria breaking up organic acids (Figure 3). (Khanal 2008b.) The bacteria can also utilize H_2 produced at a cathode or they can accept the electrons directly from the cathode, but the indirect EET via the electrochemically produced H_2 requires lower cathodic potential making it less efficient (Rabaey and Rozendal 2010). On the other hand, biofilm can improve the efficiency of the H_2 production by reducing the overpotential caused by the activation energy, which is required to induce the electrochemical production of H_2 (Jourdin *et al.* 2018; Paul *et al.* 2019; Santos *et al.* 2018 ; Rabaey and Rozendal 2010).
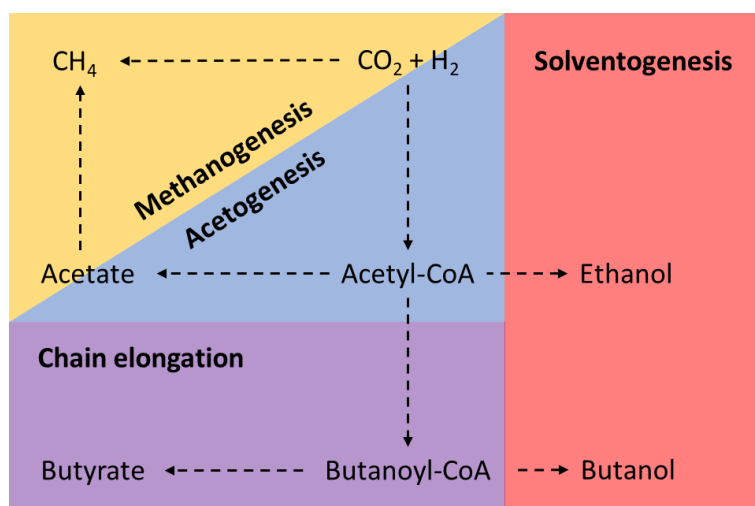
Figure 3. *Schematic of methanogenesis (yellow), homoacetogenesis (blue), chain elongation (violet) and solventogenesis (red). CO_2 and H_2 are converted into CH_4 by hydrogenotrophic methanogens and into acetate by homoacetogens, respectively. Acetotrophic methanogens can convert acetate into methane. Longer VFAs can further be produced through chain elongation and the VFAs can be turned into alcohols via solventogenesis. (Adapted from Khanal 2008b; Vassilev et al. 2018.)*

Acetogenesis coupled with MES is favourable due to the production of VFAs, which have multiple applications as plasticizer, biofuel and so forth (Jourdin *et al.* 2018). Acetate is synthesised via the Wood-Ljungdahl pathway, which goes through the acetyl coenzyme A (Acetyl-CoA) yielding acetate. The acetyl-CoA as well as acetate can be converted into longer VFAs via chain elongation or into alcohols via solventogenesis in a mixed culture (Figure 3). (Vassilev *et al.* 2018.) The electrons can also be consumed by unwanted reactions. Some heterotrophic, acetotrophic methanogens can also convert acetate into methane and back to CO_2 while the hydrogenotrophic methanogenesis competes with the acetogenesis for the same substrates (Figure 3) (Khanal 2008b).

Moreover, the acetate and methane production depend greatly on environmental factors like pH and the partial pressure of H_2 (p_{H2}). However, H_2 as well as CO_2 have low solubilities, which could limit their availability to microorganisms, and thus the efficiency and performance of MES (Bajracharya *et al.* 2016; Blanchet *et al.* 2015; Saady 2013). The concentration in the liquid phase could be increased by increasing the partial pressure, because the concentration of a gas in the liquid phase is relative to the partial pressure in the gaseous phase according to Henry's law (Sharma 2008).

The effects of the pH and the p_{H2} are illustrated in Figure 4. In MES, the conversion of CO_2 and H_2 into acetate require a high p_{H2} and prefers a neutral pH above 6, but the hydrogenotrophic methanogenesis requires a lower p_{H2} and preferably a slightly alkaline

pH (Molenaar *et al.* 2017; Vassilev *et al.* 2019). Thus in mixed cultures, the methane production can be inhibited by controlling the environmental factors (LaBelle and May 2017), but also with chemicals such as 2-bromoethanesulfonic acid (Marshall *et al.* 2012; 2013). VFAs can be further reduced into alcohols under mildly acidic (pH ~ 5) conditions (Ganigué *et al.* 2016), in addition to which Batlle-Vilanova *et al.* (2017) reported that the production of ethanol could additionally need a even higher p_{H2}. It has been suggested that acetate and ethanol can be converted into butyrate, which can further be reduced into caproate, both through reverse β – oxidation chain elongation (Batlle-Vilanova *et al.* 2017).
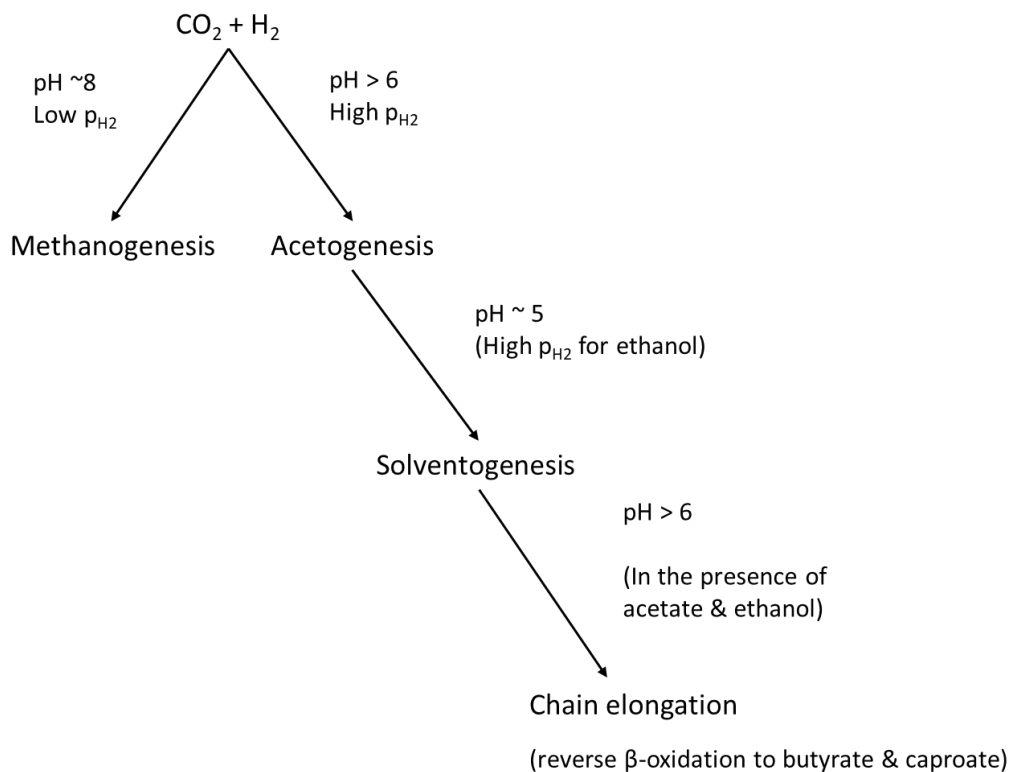
Figure 4. The effect of environmental factors into methanogenesis, acetogenesis, solventogenesis and the chain elongation. The ideal pH for methanogenesis is a mildly alkaline, but near neutral for acetogenesis. The solventogenesis prefers a pH near 5 and the ethanol production has additionally been reported to require a higher partial pressure of H_2 (p_{H2}). The chain elongation through β-reverse oxidation would also require acetate and ethanol to form butyrate and caproate.

The environmental conditions also affect the electrochemical properties of electrochemical cells and MES. Increase in the p_{H2} and pH would increase the demand for electricity, because the thermodynamic equilibrium potential (E_t) would become more negative according to Nernst equation for H_2 evolution as seen in the following equation modified from Blanchet *et al.* (2015) and Vincent *et al.* (2007).

$$E_t = E_0 - \frac{2.3 \cdot R \cdot T}{n \cdot F} \cdot (2 \cdot \text{pH} + \log(p_{H2})) \qquad (1)$$

where E_0 is the standard cathodic potential for H_2 evolution, R the gas constant, T the temperature, n the moles of electrons (2) needed to produce a mole of H_2, and F the Faraday constant (96,485 C/mol) (Blanchet *et al.* 2015; Santos *et al.* 2018; Vincent *et al.* 2007). E_0 is 0 V vs. standard hydrogen electrode (SHE) when the H_2 forms from protons (Maric and Yu 2019). In practice however, overpotential makes the onset potential of reductive reactions more negative and the onset potential of oxidative reactions more positive than the thermodynamic equilibrium potential (Paul *et al.* 2019).

1.2 Analysing bioelectrochemical systems

Multiple reactor configurations as well as operation methods from batch to continuous feeding of CO_2 or medium with varying compositions have been used making a comparison of MES results from different research groups challenging (Krieg *et al.* 2018; LaBelle *et al.* 2014; LaBelle and May 2017; Marshall *et al.* 2013). Therefore, different methods for analysing the performance of BES are used to help evaluate the results and to compare them with the literature.

1.2.1 Biological activity

The performance of the MES producing acetate or methane can be evaluated by the volumetric productivity (g/L/d), whereas in an MFC, the removal efficiency of chemicals in wastewater mirrors the productivity. One commonly used parameter regarding wastewater is the chemical oxygen demand (COD), which is the stoichiometric amount of oxygen required to oxidize the organic matter in the wastewater. (Bajracharya *et al.* 2016; Kong *et al.* 2011.)

1.2.2 Coulombic efficiency – conversion efficiency of electricity

Because of the differences between the studies, comparing e.g. the volumetric acetate productivities of different MES setups can be challenging. This can partly be solved with coulombic efficiency (CE) (Krieg *et al.* 2018), which describes the efficiency of MES to capture the electrons provided by the cathode into the product in MES (Equation 2) (Bajracharya *et al.* 2016).

$$CE = \frac{F \cdot z \cdot n_{product}}{\int I_{consumed} \cdot dt} \cdot 100 \% \qquad (2)$$

where z is the number of electrons stoichiometrically needed to form n moles of the product and $I_{consumed}$ is the current supplied over a time period dt also known as charge. (Bajracharya *et al.* 2016; Krieg *et al.* 2014.) The stoichiometric number of electrons required to produce acetate and butyrate are 8 electrons and 20 electrons according to Equations (3) and (4), respectively.

$$2\ CO_2 + 8\ e^- + 7\ H^+ \rightarrow C_2H_3O_2^- + 2\ H_2O \tag{3}$$

$$4\ CO_2 + 20\ e^- + 19\ H^+ \rightarrow C_4H_7O_2^- + 6\ H_2O \tag{4}$$
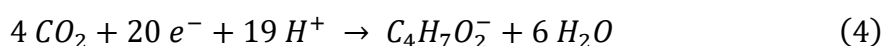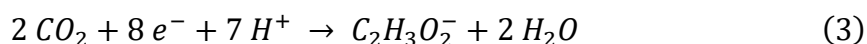
Equation (2) is inverse in the case of MFC (Equation 5), where the CE reflects the number of electrons used in generating a current versus the electrons available in the organic compounds (Krieg *et al.* 2014).

$$CE\ in\ MFC = \frac{\int I_{produced} \cdot dt}{F \cdot z \cdot n_{substrate}} \cdot 100\ \% \tag{5}$$

1.2.3 Cyclic voltammetry – electrochemical properties

The electrochemical properties such as overpotential of a BES reactor affect the bioelectrochemical reactions. Cyclic voltammetry (CV) is used to determine onset potential or overpotential for a reaction in a given system (Li *et al.* 2018). To run a CV, a reference electrode with a known potential is placed close to the working electrode. A potentiostat is used to scan potentials and record the resulting currents at the working electrode in one direction and back to make at least one cycle. (Logan *et al.* 2006.) The potentials are then plotted against the resulting currents in a voltammogram, in which the onset potential is the potential, after which the current starts a more rapid decrease or an increase in reductive or oxidative reactions, respectively (Li *et al.* 2018; Logan *et al.* 2006; Paul *et al.* 2019).

1.2.4 Polarization curve – generated power density

Similar to a CV, a polarization curve shows the relationship of a potential to a current, and it can be used to calculate the maximum achievable electric power in MFC. The polarization curve can be run with a potentiostat or with a variable resistor, which is used to change the external resistance and to measure the resulting voltage. According to Ohm's law, the current and the power can be calculated when the resistance and the voltage are known. (Logan *et al.* 2006.)

1.3 Bioelectrochemical reactor parameters

One of the challenges in the research about BESs is the lack of standardized reactor systems. Because of limited number of readily available reactors suitable for bioelectrochemical applications, the majority of the bioelectrochemical cells used are custom-made or modified commercial bioreactors. (Krieg *et al.* 2018.) However, all the electrochemical systems have at least a working electrode and a counter electrode, and usually a semi-permeable separator as seen in Figures 1 and 2. In three-electrode cell systems, a reference electrode is placed close to the working electrode to enable applying or recording a known potential (Krieg *et al.* 2014).

1.3.1 Electrode material

Electrode properties are important in electrochemical cells as well as in BES for the redox reactions and the interaction between the bacteria and the electrodes. In addition to being good conductors (Krieg *et al.* 2018), the electrode should be cheap, support cell growth and be nontoxic to the bacteria (Sharma *et al.* 2019). The material should also have a high surface to volume ratio (SVR) for sufficient mass transfer and to endorse the formation of biofilm necessary for the direct EET, which promotes the performance of BES (Dong *et al.* 2018; Jourdin *et al.* 2016; Kracke *et al.* 2015; Krieg *et al.* 2018).

While metals may be good conductors, they can be expensive in larger quantities as the material for the biotic electrode. However, smaller pieces of metal can be used as the current collectors that conduct electricity to cheaper electrode materials like carbon, which is conductive, cheap and biocompatible. (Krieg *et al.* 2018; Sharma *et al.* 2019.) Carbon as an electrode material is also diverse; it has been deployed as rods, felts and granules, some of which can be seen in Table 1.

Table 1. *The effect of carbon-based electrode material on the acetate production in MES. Volumetric productivities and coulombic efficiencies of acetate achieved using different materials in a batch or a semi-batch cultivation in the literature. The semi-batch in here is a batch with continuous or regular supply of CO_2.*

Electrode	Productivity (g/L/d)	CE[a] (%)	Operation	Paper
4 g/L GAC[b] + carbon felt	0.10	63	Semi-batch, 24 days	(Dong *et al.* 2018)
16 g/L GAC[b] + carbon felt	0.14	65	Semi-batch, 24 days	(Dong *et al.* 2018)
400 g/L graphite granules + 9.0 cm^2 graphite rod	0.24 (max)	N/A	Semi-batch, 10 days	(Marshall *et al.* 2012)
10 cm^2 graphite rod	0.22 (max)	40 (max)	Batch, 4 days	(LaBelle *et al.* 2014)
1000 g/L graphite granules + 2 cm^2 graphite rod	3.1 (max)	N/A	Semi-batch, 20 days	(LaBelle *et al.* 2014)
37 cm^2 multiwalled nanotube with reticulated vitreous carbon	0.37	99	Batch with HCO_3^- additions, 63 days	(Jourdin *et al.* 2016)

[a]Abbreviation: CE, Coulombic efficiency. [b]Abbreviation: GAC, Granular activated carbon.

In some studies, the increased total area of the cathode improved the performance of MES resulting in higher acetate production as can be seen in the Table 1. LaBelle *et al.* (2014) and Marshall *et al.* (2012) reported higher volumetric production rates when the amount of graphite granules and/or the area of the graphite rod was increased. Additionally, Dong *et al.* (2018) observed that increasing the amount of granular activated carbon (GAC) at the cathode increased the acetate concentration produced. Because the volume was constant with all the GAC concentrations, the volumetric productivity also increased with increasing GAC concentration. Jourdin *et al.* (2016) reported an even higher volumetric production rate with a highly porous cathode than what was reported with the graphite materials and the GAC listed in Table 1. Though increasing the surface area of the cathode may not always improve the production and performance due to the electrode properties or other limitations (Bajracharaya *et al.* 2016; Jourdin *et al.* 2016).

To improve the bioavailability and the mass transfer of continuously fed CO_2, Bajracharya *et al.* (2016) used a gas diffusion electrode (GDE) as the cathode in MES. The maximum production rate reached was 0.24 g/L/d, which is similar to the 400 g/L of the graphite granules and the graphite rods seen in Table 1, but lower than, what for instance Jourdin *et al.* (2016) observed with a high SVR cathode. Bajracharya *et al.*

(2016) noted that CO_2 was not the limiting factor for the acetate production, but rather the other factors such as the availability of the electrons, because the production rate was lower than what it could theoretically have been with the CO_2 supply.

1.3.2 Separators

In MES, the diffusion of oxygen from the anode to the cathode could be detrimental to the obligatory anaerobic acetogens, but it could also cause an electron loss by unwanted reactions or enable microbial aerobic break down (oxidation) of the products (Batlle-Vilanova *et al.* 2017; Blanchet *et al.* 2015; Vassilev *et al.* 2018). To avoid this and possible short circuits, the anode and the cathode need to be separated (Krieg *et al.* 2018).

BES reactors can be roughly divided into two categories based on the separation: single-chamber and two-cell reactors. In single-chamber reactors, the electrodes are in the same space, while in the two-chamber reactors, the electrodes are separated with a selective separator that still allows the diffusion of ions from the anode to the cathode. In the single-chamber reactors, the unwanted mixing of the products can be avoided by increasing the distance between the working and counter electrodes, but this increases the internal resistance. However, the electric resistance of separators such as ion exchange membranes (IEM) can increase the internal resistance as well, but a separator also enables shorter distance between electrodes, which in turn reduces the internal resistance. (Krieg *et al.* 2018.)

IEMs are important to achieve the production of acetate and other VFAs at high rates with high efficiencies. They include anion exchange membranes (AEM), proton exchange membrane (PEM) and cation exchange membranes (CEM), which allow a selective migration of anions, protons and cations, respectively (Gildemyn *et al.* 2017; Krieg *et al.* 2018; Krieg *et al.* 2014). Because acetate is negatively charged, it would migrate to the anode, if the sole separator between the electrodes was an AEM (Gildemyn *et al.* 2017). However, Gildemyn *et al.* (2017) added an AEM between the CEM and the cathode for the simultaneous extraction of acetate. They observed a higher production and efficiency, because the acetate levels stayed below inhibitory levels at the cathode (Gildemyn *et al.* 2017). Furthermore, Vassilev *et al.* (2019) utilized a similar CEM-AEM combination to introduce a second cathode chamber separated by an AEM from the first cathode chamber. The pH could be low enough for simultaneous solventogenesis in the second

cathode chamber while still having the optimal pH for acetogenesis and chain elongation in the first cathode chamber.

1.4 Reactor models applied in microbial electrosynthesis to produce acetate

1.4.1 Concentric tubular reactor

Possibly the first reported BES reactor was a concentric tubular reactor, where Potter (1911) introduced yeast *Saccharomyces cerevisiae* and observed a current being generated. In concentric tubular reactors, a cylindrically shaped container is placed inside an outer tubular reactor, which contains the opposite electrode. The cylinder either has an opening for a semi-permeable separator or the cylinder itself is completely made from a porous or semi-permeable material such as an IEM. (Figure 5) (Batlle-Vilanova *et al.* 2017; Krieg *et al.* 2018; Potter 1911; Vassilev *et al.* 2018.)
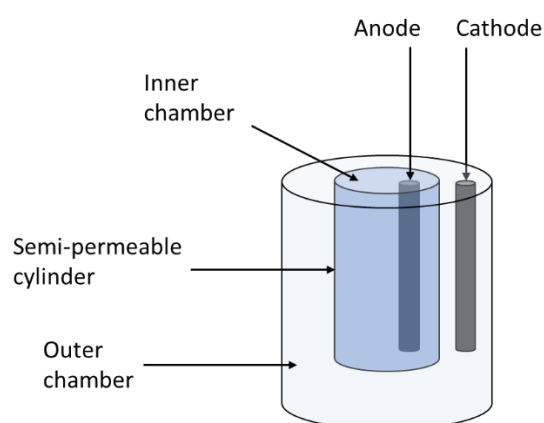
Figure 5. *A concentric tubular reactor. The cylinder (darker blue) separating the outer and inner chambers can be completely semi-permeable, or a semi-permeable window can be introduced onto the cylinder. The anode can be in the inner chamber and the cathode in the outer chamber or reverse. (Adapted from Krieg et al. 2018.)*

A concentric tubular reactor is relatively adaptable in terms of sizing and operation methods. To test the effect of the porosity level of the cathode on the performance of MES, Jourdin *et al.* (2016) built a concentric tubular reactor in a bottle, where a small compartment for the anode was added, resembling the reactor in Figure 5 (Jourdin *et al.* 2016). Batlle-Vilanova *et al.* (2017) constructed a bigger reactor, where the inner chamber was inside a tubular CEM hosting a carbon cloth, which served as the cathode. The medium was recirculated through the tubular cathode chamber from the bottom to the top. Vassilev *et al.* (2018) constructed a similar reactor with graphite granules serving as the cathode in the outer chamber.

15

Batlle-Vilanova *et al.* (2017) and Vassilev *et al.* (2018) operated the reactors at mildly acidic pH to produce longer VFAs than acetate. Batlle-Vilanova *et al.* (2017) reported the maximum butyrate production of 0.16 g/L/d, which is more than double the 0.07 g/L/d reported by Vassilev *et al.* (2018). Additionally, both systems produced ethanol and butanol, although even longer VFAs and alcohols were also produced in the latter case (Batlle-Vilanova *et al.* 2017; Vassilev *et al.* 2018).

1.4.2 H-cell reactor

Some of the simplest two-chambered reactor models include the H-cell reactor, which consists of two bottles conjoined together in an H-shape. By mounting a membrane between the two bottles, the reactor is divided into anode and cathode chambers, but long distance between the electrodes can negatively affect the performance (Figure 6). The media in the chambers are mixed with magnetic stirrers. (Krieg *et al.* 2018.)
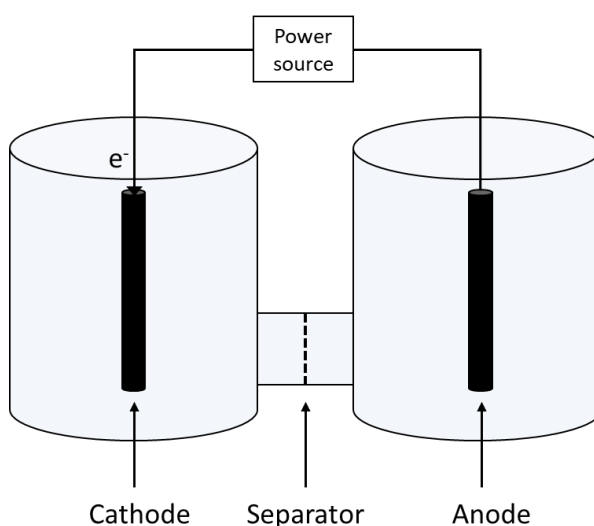
Figure 6. *An H-cell reactor (Adapted from* Krieg *et al.* 2018*).*

However, an H-cell is easy to assemble and it has been used to study simple variables such as electrode materials and electroactive bacteria (Dong *et al.* 2018; Krieg *et al.* 2018; Nevin *et al.* 2010). For example, the graphite granules and the GAC mentioned in Table 1, were tested in H-cell reactors (Dong *et al.* 2018; LaBelle *et al.* 2014; Marshall *et al.* 2012).

1.4.3 Other two-chambered reactors

In addition to the relatively easily classifiable and recognizable concentric tubular and H-cell reactors, a range of scalable two-chambered reactors have been developed. These reactors have been built in the labs from different materials with varying dimensions and

shapes. (Bajracharya *et al.* 2016; Jourdin *et al.* 2018; Krieg *et al.* 2018; LaBelle and May 2017.)

Compared to H-cell reactors, the electrodes can be positioned closer to the membrane and each other in flat plate reactors like in Figure 2B (Jourdin *et al.* 2018; Krieg *et al.* 2018; LaBelle and May 2017). LaBelle and May (2017) and Jourdin *et al.* (2018) operated flat plate reactors in continuous mode increasing the productivity: they reported maximum acetate productivities of 18.7 and 9.8 g/L/d, respectively.

In cube-type reactors, cylindrical compartments are carved into two cubes, which are mounted together with a membrane between them to create two cylindrical chambers (Figure 7) (Krieg *et al.* 2018). To study the GDE Bajracharya *et al.* (2016) built and tested a similar reactor from cylindrical rings reaching to the maximum acetate production rate of 0.24 g/L/d with continuous CO_2 supply.
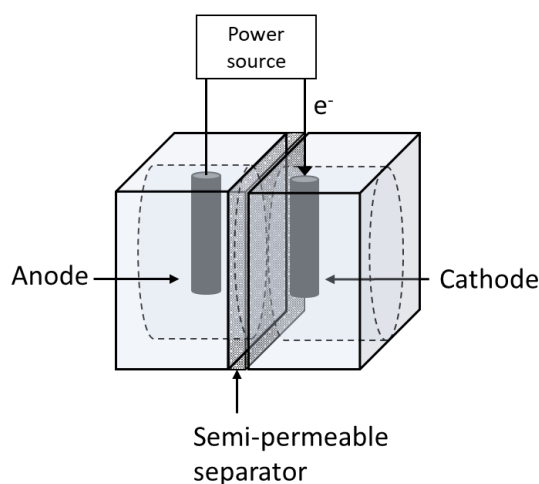
Figure 7. *A cube-type reactor. The chambers are cylinders inside a cube. (Adapted from Krieg et al. 2018.)*

1.5 Improved reactor configurations

Acetate production of MES has been improved, but even when the acetate productivity reached as high as 18.7 g/L/d, the production costs together with extraction and purification could have exceeded the market price making it unprofitable (LaBelle and May 2017). More valuable compounds and further increase in productivity and efficiency of MES with lower production costs are needed to make MES profitable, competitive and applicable to an industrial scale (LaBelle and May 2017; Marshall *et al.* 2013; Vassilev *et al.* 2018). In addition to the operation, the reactor also has a great impact on the performance (Krieg *et al.* 2018), and therefore, the economic efficiency could be improved with reactor design.

1.5.1 Fixed bed reactors

A bed reactor contains particulate or granular material as the catalytic bed, yielding a high SVR and consequently increased reactive area and reaction rate. In fixed bed reactors (FixBR) the bed remains settled in a "fixed" position inside of a typically tubular reactor while a fluid is passed through the bed to ensure mixing (Figure 8A). The bed material serves as the catalyst, but also as the support material for microbial growth in cases of biological FixBRs. (Bello *et al.* 2017; Li *et al.* 2013; Rabaey *et al.* 2005; Worstell 2014).
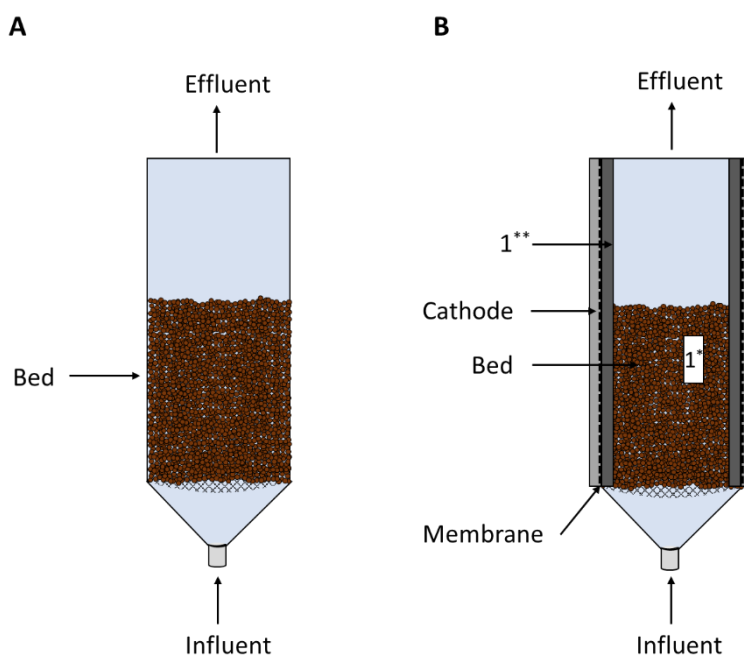
Figure 8*. (A) A basic fixed bed reactor (FixBR). (B) A FixBR modified into a two-chamber microbial fuel cell (MFC), where the tubular anode chamber is inside the cylindrical cathode chamber and hosts the bed electrode. Li et al. (2013) used a titanium mesh tube (1**) while Rabaey et al. (2005) used a graphite rod (1*) as the current collector for the bed at the anode. (Adapted from Li et al. 2013; Rabaey et al. 2005).*

In bioelectrochemical FixBRs, the bed material also serves as the electrode (Quejigo *et al.* 2019), thus the bed should also be conductive. As seen in Table 1, the graphite granules and the GAC in the H-cell reactors supported acetate production via MES, so they could have potential in FixBR-MES combinations. Additionally, LaBelle *et al.* (2014) sparged CO_2 continuously into the cathode chamber filled with the granules, hence the setup might have been a FixBR, although not a typical one as defined by Worstell (2014).

Tubular up-flow FixBRs have been adapted MFC applications, where wastewater has been passed through the fixed bed. Rabaey *et al.* (2005) and Li *et al.* (2013) constructed two-chambered FixBR-MFC combinations, which resembled concentric tubular reactors, where the inner chamber was a tube filled with the bed material serving as the anode. As

seen in Figure 8B, Li *et al.* (2013) also added a rolled graphite felt as part of the anode and a titanium mesh roll between the membrane and the felt to serve as the current collector while Rabaey *et al.* (2005) embedded a graphite rod in the bed as the collector.

Rabaey *et al.* (2005) observed that FixBR could be used in MFC to produce electricity and to treat wastewater. Since then FixBR-MFC combinations have been further studied and improved. Li *et al.* (2013) and He *et al.* (2015) reported higher removal of COD with different wastewaters, although the power densities were significantly lower than 48 W/m^3 reported by Rabaey *et al.* (2005).

The bed of porous particles provides a higher SVR, hence possibly improves the biofilm formation and increases the electrode surface area interacting with the electroactive bacteria (Sharma *et al.* 2019). Regarding MES, FixBR might also provide another advantage by increasing the level of dissolved H$_2$ produced at the cathode. According to a hypothesis, H$_2$ is formed as dissolved H$_2$ at the cathode before it transfers into gas phase after reaching its maximum solubility (Trinke *et al.* 2017). However, poorer mixing of phases in FixBR can limit the liquid-to-gas transfer, which promotes the dissolved H$_2$ to exceed its maximum solubility and to supersaturate (Castelló *et al.* 2020). Subsequently, FixBR might increase the bioavailability of H$_2$ and thus the bioelectrochemical acetate production (Battle-Vilanova *et al.* 2017; Patil *et al.* 2015).

Nevertheless, FixBRs have some disadvantages. The limited mass transfer can create temperature gradients, and excessive microbial growth can clog the bed creating dead zones (Castelló *et al.* 2020; Bello *et al.* 2017). Due to the distances between the granules and the current collector, the distribution of the potential across a bed electrode can be heterogenous resulting in a higher internal resistance and possibly affecting bioelectrochemical reactions (Hiddleston and Douglas 1970; Quejigo *et al.* 2019).

1.5.2 Fluidized bed reactors

The setup of a fluidized bed reactor (FluBR) resemble that of a FixBR, but the solid bed is fluidized with an adequate superficial velocity (volumetric flow rate divided by the cross-section) of a gas or liquid through the bed. Increasing the velocity increases the bed height, until the fluidization velocity exceeds the maximum velocity causing the particles to escape the reactor. (Bello *et al.* 2017.)

Fluidization causes the particles to move and behave more like a fluid, which ensures better heat distribution and higher mass transfer rates. The movement of the particles reduces biomass clogging and fouling of a membrane due to the particles rubbing against

the membrane. (Bello *et al.* 2017.) Because FluBRs have improved biological wastewater treatments and pollutant removal treatments (Bello *et al.* 2017), they could benefit BES. However, the distance between the particles and the current collector would be further increased when the bed is fluidized, which could potentially reduce the conductivity (Hiddleston and Douglas 1970; Kim and Kang 1997; Quejigo *et al.* 2019).

Although FluBR has not yet been reported in MES applications, Dong *et al.* (2018) fluidized varying concentrations of GAC with a magnetic stirrer in an H-cell reactor. However, due to the experimental setup, the improved performance was attributed to the higher surface area when the amount of GAC was increased. Dong *et al.* (2018) did not describe a control for fluidization that would have provided the same surface area with as good mixing without fluidization, thus the benefits of fluidization itself are unclear.

FluBRs have been applied in MFC. Huang *et al.* (2011) and Gao *et al.* (2019) combined MFC and FluBR, where a tube hosts the anode bed material and has an opening to a cathode chamber separated from the anode with a membrane (Figure 9). Kong *et al.* (2011) built an otherwise similar tubular one-chamber FluBR-MFC but without a membrane and with an air-cathode attached to the perforated reactor wall.
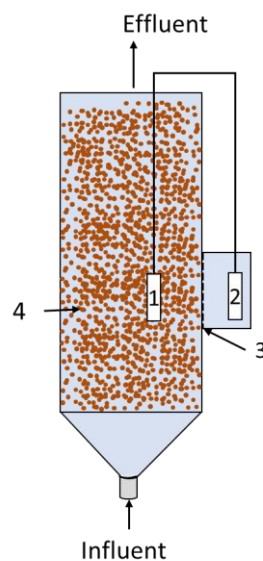
Figure 9. *Examples of fluidized bed reactors (FluBR) combined with a microbial fuel cell (MFC) (1. Anode/Current collector 2. Cathode 3. Membrane 4. Bed). FluBR-MFCs built by Huang et al. (2011) and Gao et al. (2019) had a tubular anode chamber with a window for a cathode compartment (Adapted from Huang et al. 2011).*

Kong *et al.* (2011) reported higher maximum power densities in a single-chamber FluBR-MFCs, than what Gao *et al.* (2019) and Huang *et al.* (2011) reported in two-chamber setups (Table 2). The single-chambered FluBR-MFCs and their bed-free control produced

the high maximum power densities possibly due to decreased internal resistance in the absence of a membrane (Kong *et al.* 2011; Krieg *et al.* 2018). On the other hand, the maximum power densities were calculated from polarization curves (Kong *et al.* 2011), hence they are the highest achievable power densities. The treated wastewaters also differed between the studies, which could have affected the performance (Gao *et al.* 2019; Huang *et al.* 2011; Kong *et al.* 2011).

Table 2. *Performance of fluidized bed microbial fuel cell reactors. The power density is normalized to the anode surface area.*

Bed material	Anode chamber volume (L)	Maximum power density (mW/m^2)	Removal of COD[a]	Reference
17 % (v/v) PPC[b]	10.7	35.4	98.6	(Gao *et al.* 2019)
10 % (v/v) PPC[b]	7.27	120	80 – 90	(Huang *et al.* 2011)
100 g GAC[c]	0.75*	400**	86	(Kong *et al.* 2011)
100 g graphite granules	0.75*	540**	79	(Kong *et al.* 2011)
no bed material	0.75*	240**	50	(Kong *et al.* 2011)

*Calculated from dimensions. **Original author determined from polarization curves. [a]Abbreviation: COD, Chemical oxygen demand. [b]Abbreviation: PPC, porous polymer carrier. [c]Abbreviation: GAC, granular activated carbon.

Kong *et al.* (2011) reported higher COD removal efficiencies with the bed materials compared to the bed-free control, which could have been due to the higher biomass and its enhanced activity. However, the amounts of the GAC and the graphite granules were the same, but the 340 times higher specific surface area ($A_{specific}$) of the GAC did not improve the power density and increased the COD removal by only a few percent (Table 2). On the other hand, according to Kong *et al.* (2011), the electric resistance of the GAC was higher than the resistance of the graphite granules, which could have increased the power density in the reactor with the graphite granules.

Although, the power densities were high in the FluBR-MFC configurations, higher densities have been reported with other MFC configurations. Using a tubular activated carbon fiber felt in a tubular MFC reactor, Deng *et al.* (2010) determined a maximum power density 784 mW/m^2 from a polarization curve. Though the methods and the wastewaters were not the same, which could have affected the results (Deng *et al.* 2010; Gao *et al.* 2019; Huang *et al.* 2011; Kim and Kang 1997; Kong *et al.* 2011). Additionally, similar to the study by Dong *et al.* (2018), there were no controls for fluidization that would have provided as good mixing with similar-sized bed particles but without fluidization under otherwise identical conditions (Gao *et al.* 2019; Kong *et al.* 2011).

The effect of FluBR into MES performance needs to be studied. To gain more insight, the objective of this Master's thesis was to test the effect of FluBR on the production of acetate from CO_2 in MES and a similar FixBR was constructed as a control.

2 Materials and methods

2.1 Media

The culture medium (2.1 g 2-bromoethanesulfonate 8.5 g Na_2HPO_4; 3 g KH_2PO_4; 3 g NH_4Cl; 1 g yeast extract; 15 mg $CaCl_2$; 9.8 mg $MgSO_4$; 10 mL trace element solution and 1 mL vitamin solution per litre) used in the biotic reactors contained 2-bromoethanesulfonate to inhibit methanogenic activity at the cathode. The trace element and vitamin solutions were prepared as described in the DSMZ medium 141 for *Methanogenium* strains. The minimal medium for the abiotic reactors was prepared in the same way as the medium for biotic experiments, but the vitamin solution and the yeast extract were left out to prevent the growth of microorganisms at the cathode chambers in the abiotic reactors. The medium for the anode chamber in all the reactors comprised 6 g/L Na_2HPO_4.

2.2 Microbial culture and inoculation

The inoculum was attained from the Faculty of Engineering and Natural Sciences in Tampere University. The uncharacterised mixed culture from a cow's rumen was enriched in a bioelectrochemical system for ca. 5 months, during which it was fed with CO_2 as the sole carbon source and electricity as the sole energy source.

Oxygen was removed from the media by sparging it with N_2 for at least an hour before transferring the medium into the cathodic recirculation bottle, where it was sparged with CO_2 for ca. $30 - 60$ min before filling the cathode chamber. The bioFixBR and the bioFluBR were inoculated to the initial optical densities (OD_{600nm}) of 0.23 and 0.25, respectively, in the total volume of 800 mL. The working volume in the abiotic reactors was also 800 mL. After inoculation, the biotic FixBR (bioFixBR) and the biotic FluBR (bioFluBR) were operated for 30 and 33 days, respectively. The abiotic FixBR (abioFixBR) and the abiotic FluBR (abioFluBR) were operated for 6 and 7 days after a CV, respectively. The reactors were kept at ca. 35 ºC.

2.3 CO_2 feeding and sampling

After inoculating the biotic reactors, a sample was taken to measure the OD_{600nm} and the initial VFA content, while the abiotic reactors were sampled only to measure the initial

VFA content after the CV. The bioFluBR was resampled 0.25 days after the inoculation to get a more representative sample for the initial pH, OD_{600nm} and VFA concentration.

Every 1 – 4 days liquid samples were taken from the cathode chamber to measure the pH and the VFA content in the abiotic tests while the pH, the VFA content and the OD_{600nm} were measured from the biotic experiments. After sampling the microbes were fed with CO_2, which also decreases the pH as the dissolved CO_2 reacts with water to form carbonic acid (Vassilev *et al.*2018). The cathode recirculation bottles were sparged with CO_2 for 15 – 30 min or until the pH was between 6 and 7. The flow rate of CO_2 was kept between ca. 0.16 and 0.32 mL/min with a rotameter (Kytölä, Finland).

2.4 Reactor setup & operation

To test the effect of the bioFixBR and the bioFluBR on acetate production from CO_2, two up-flow two-chamber reactors were built and set up. To rule out the possibility of acetate production without biomass, abiotic controls were also done for both reactors.

A cylindrical anode chamber (approximately 110 mL) and a tubular cathode chamber (200 mL) were separated by a 116.6 cm^2 CMI-7000S membrane (Membranes International, United States) (Figure 10C), which was remodelled into a tubular shape with an inner diameter (ID) of 3.1 cm using 3D printed parts (polyethylene terephthalate glycol) (Figure 10A). The reactor was composed from four acrylic glass parts (Figure 10B), creating a cathodic chamber, where the ID of the top half was approximately 3.2 cm. The cathode chamber inlet (ID = 0.8 cm) was at the bottom of part 1, which was a cone filled with glass beads (Ø = 6 mm) to ensure uniform flow of medium to the reactor. Part 2 was placed on top of the cone and a titanium mesh (18 mesh woven from 0.28 mm diameter wire, Alfa Aesar, Germany) was fastened between the parts 1 and 2 as cathodic current collector. The membrane was secured into its place by fastening part 3 on top of the part 2, and the reactor was completed with part 4, which was a flat disk with three outlets on top of the reactor (Figure 10B).
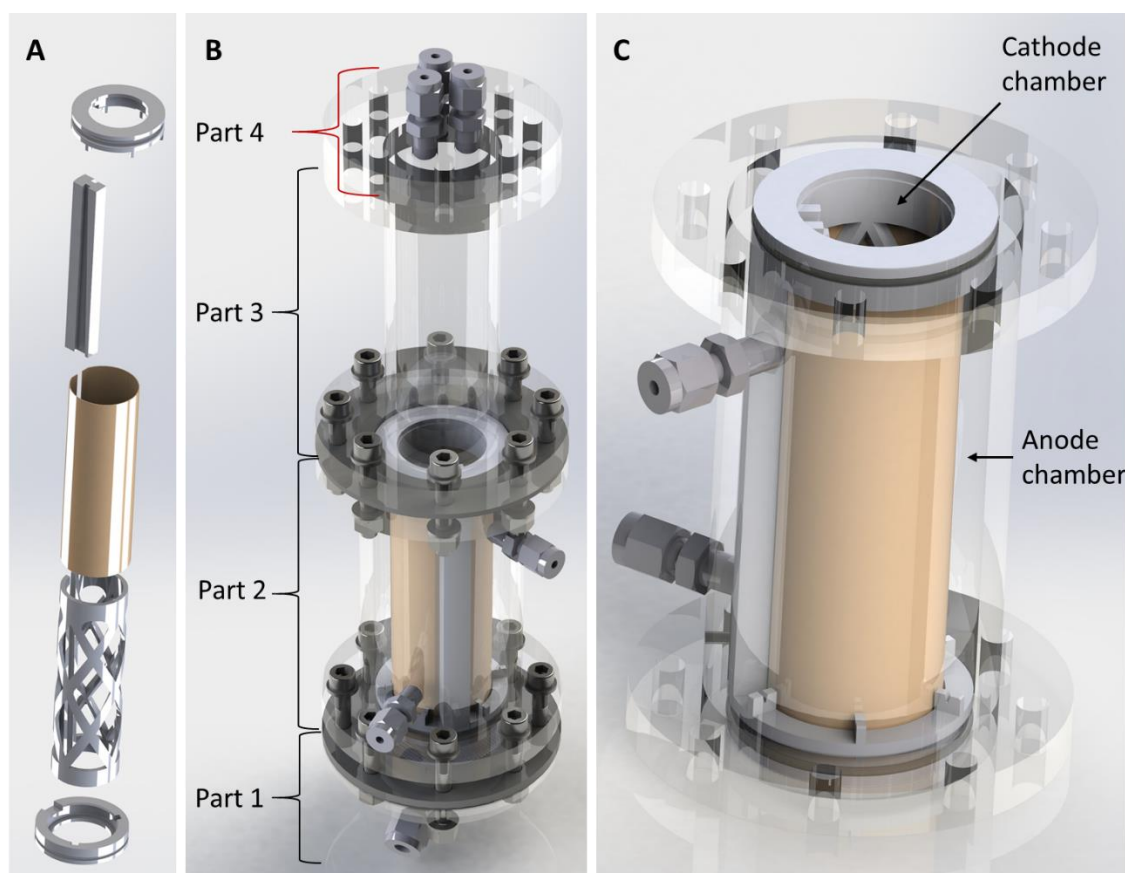
Figure 10. *The two-chamber tubular reactor. (A) The membrane was reshaped in tubular form with a holder, which was placed inside (B) the reactor consisting of parts 1, 2, 3 and 4. (C) In the part 2, the membrane created the tubular cathodic chamber surrounded by the cylindrical anode chamber. Drawings by Mika Karttunen with Solidworks (Dassault Systémes Solidworks, France).*

To make the cathode gas- and watertight, two rubber gaskets covered with Vaseline were added between each part. At the cathode, the titanium mesh served as a current collector, which charged the carbon-based material above. In FluBR 30 g (29.5 mL) of more easily fluidizable GAC with a diameter of ca. 1.3 mm (Cyclecarb 305, Chemviron, Belgium) served as the bed material, while 55 g of EC-100 graphite granules with a diameter up to 10 mm (Graphite Sales, the USA) were added in FixBR. As the anode electrode, a 12 cm platinum wire (0.4 mm diameter, Advent Research Materials Ltd, Great Britain) was positioned on the bottom of the anodic chamber, around the membrane. An Ag/AgCl reference electrode (3 M NaCl, MF-2052, Bioanalytical Systems, the USA) in a glass tube with a frit (QiS, the Netherlands) filled with 3 M NaCl was placed under the mesh. The potentials vs. Ag/AgCl in 3 M NaCl are converted into V vs. SHE by adding +0.21 V (Siegert 2018) and the potentials mentioned hereafter are in V vs. SHE.

2.4.1 Fluid recirculation and its optimization

The liquid chamber contents were recirculated with Masterflex peristaltic pumps (Cole-Parmer, United States). The content of the anodic chamber was recirculated at the flow rate of 44 ± 0.1 mL/min, while the cathodic chamber content was recirculated at approximately 250 ± 4 mL/min in the bioFixBR, the abioFixBR and the abioFluBR. In the bioFluBR, the flow rate was 170 ± 4 mL/min to overcome issues with the pump. However, the pump head had broken, which was noticed and replaced ca. 5 hours after inoculation to ensure proper medium-mixing in the bioFluBR. The level of fluidization or the increase in the bed height was not measured in the abioFluBR, but in the bioFluBR it was measured to be 8.05 ± 0.41 cm which equals a 7 % increase.

Three-way valves were added between the pumps and the recirculation bottles in the anodic and cathodic recirculation loops for sampling (Figure 11). Because the cathode recirculation bottles were sparged with CO_2 via the same port, the recirculation had to be stopped while sparging, but the current was still applied at the cathode to produce H_2. When the recirculation was turned on again and the flow rate was increased, gases escaped the cathode chambers as bubbles. In the bioFluBR and the abioFluBR, those bubbles carried GAC into the recirculation bottle.
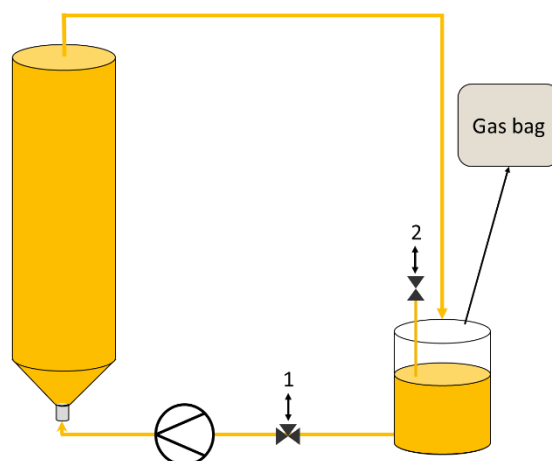
Figure 11. *The cathodic liquid recirculation of the reactors. In the biotic fixed bed reactor (bioFixBR) and the abiotic reactors, the sample valve (1) was within the recirculation loop between the pump and the recirculation bottle. In the biotic fluidized bed reactor (bioFluBR), the valve was removed and a separate sampling port (2) was added into the bottle to allow continuous recirculation, while sparging the recirculation bottle with CO_2.*

Hoses detached below the cathode chamber inlets in the early setups of bioFluBRs possibly because of blockages caused by the recirculating GAC. To overcome the issue, the recirculation loop and the reactor outlets of the bioFluBR were modified; the valve

was removed from the cathodic recirculation loop and a separate port for sampling and CO_2 sparging was added directly into the recirculation bottle to allow continuous recirculation while sparging with CO_2 (Figure 11). The differences in the reactors can also be seen in Figure 12.
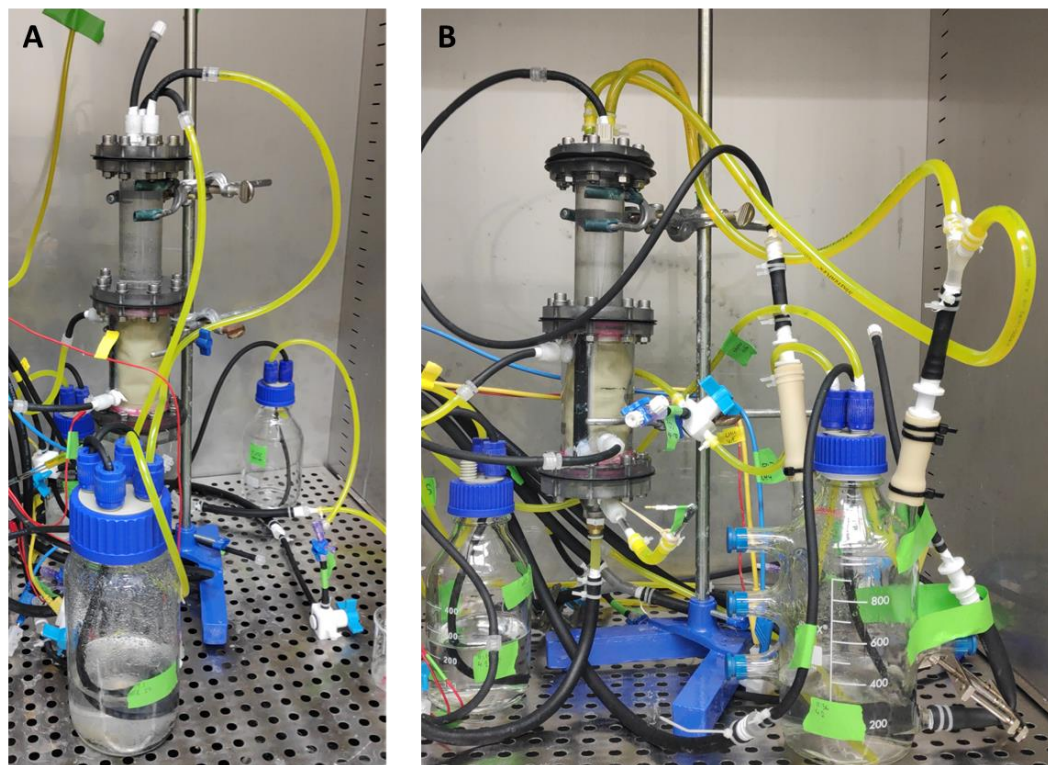
Figure 12. *(A) The abiotic fluidized bed reactor (abioFluBR) compared with (B) the biotic fluidized bed reactor (bioFluBR) built. The recirculation loops were the same in the abiotic reactors and the biotic fixed bed reactor (bioFixBR). The 500 mL bottle in the A picture is not connected to the abioFluBR.*

2.4.2 Electric connections

The reactor was a three-electrode cell, where the Ag/AgCl electrode functioned as the reference, the cathode as the working electrode and the anode as the counter electrode. The electrodes were connected to a multichannel potentiostat (VMP-3, BioLogic Science Instruments, France), which was used to control the potential (chronoamperometry) or the current (chronopotentiometry) at the working electrode.

Before inoculation, the reactors were stabilized for 16 – 19 h. The bioFixBR was stabilized by fixing the potential to –1.01 V while the potential and the resulting current were recorded every 100 s. After inoculation, the potential was first fixed to –0.69 V, but 0.7 days after inoculation, it was decreased to –0.74 V to reach negative enough current at the same potential with both granule types. To overcome the difference in the H_2

formation overpotential between the FixBRs and the FluBRs, the operation mode was switched into chronopotentiometric mode 7 days after inoculating the bioFixBR. In the chronopotentiometric mode, the current was fixed to –70 mA while the current and the resulting potential were recorded every 100 s. The rest of the reactors (bioFluBR, abioFluBR and abioFixBR) were stabilized and operated chronopotentiometrically from the beginning.

2.5 Analyses

2.5.1 Cyclic voltammetry

CV was run to see where the H_2 production starts with the abiotic reactors (Blanchet *et al.* 2015; Paul *et al.* 2019). Before running the first CV at the beginning of each batch (before inoculation) the pH was decreased to 6.7 with CO_2. Another CV was performed at the end of the abioFluBR and the abioFixBR to see, if the onset potential or overpotential changed. The current was recorded in response to the applied potential at the rate of 1 mV/s. Each CV consisted of three repetitions between the potential ranges listed in Table 3. Because of overloads, the CV range was changed between the reactors (Table 3).

Table 3. *The potential range of the cyclic voltammetries.*

Granules	Reactor	Before batch	After batch
GAC[a]	bioFluBR[b]	from –0.39 to –1.09 V	N/A
	abioFluBR[c]	from –0.39 to –1.09 V	from –0.39 to –0.94 V
Graphite	bioFixBR[d]	from –0.54 to –0.84 V	N/A
granules	abioFixBR[e]	from –0.39 to –1.02 V	from –0.39 to –0.94 V

[a]Abbreviation: GAC, Granular activated carbon. [b]Abbreviation: bioFluBR, biotic fluidized bed reactor. [c]Abbreviation: abioFluBR, abiotic fluidized bed reactor. [d]Abbreviation: bioFixBR, biotic fixed bed reactor. [e]Abbreviation: abioFixBR, abiotic fixed bed reactor.

The CVs were performed with the recirculation on, but the pump head may have been broken already before the CV used in the bioFluBR (data not shown), which potentially hindered mixing while adjusting the pH with CO_2 and during the CV. The voltammogram of the bioFixBR is also not shown.

2.5.2 Analysing volatile fatty acid content

The VFA content was measured with a Shimadzu GC-2010 Plus Capillary gas chromatography (GC) with AOC-20i autoinjector (Japan) equipped with a flame

ionization detector and a ZB-WAX plus column (Phenomenex, United States) as described by Haavisto *et al.* (2017).

For the VFA analysis, the samples were filtered (Ø = 0.2 µm) and stored at –20 ºC prior to the analysis. The standards contained 0.5 – 10 mM of alcohols (ethanol and butanol) as well as 0.5 – 10 mM of acetate, propionate, butyrate, isobutyrate and valeric acid. The internal standards and the acidification agent were added according to Haavisto *et al.* (2017).

2.6 Calculations

To evaluate the performance of the reactors, the CE and the volumetric productivities were calculated. The CE was calculated according to Equation 2 and the productivity of acetate in g/L/d was normalized to the volume of the cathode medium. To calculate the current density of the cathode the current was divided by the projected surface area of the membrane.

3 Results

3.1 Abiotic reactors

The abiotic reactors were tested to demonstrate, if CO_2 could be electrochemically catalysed into producing acetate in the absence of biomass. The abioFixBR and the abioFluBR did not produce acetate or other VFAs. Water was likely electrolysed into O_2 at the anode and H_2 at the cathode, but gases were not analysed.

3.1.1 Cyclic voltammetry

The CVs were performed to find out the onset potential for H_2 production (Li *et al.* 2018). According to the voltammogram before the batch, the current became more notable below –0.80 V, reaching a current of –100 mA at –1.09 V in the abioFluBR (Figure 13A). In the abioFixBR, the current became more notable below –0.70 V, reaching ca. –130 mA at –1.02 V (Figure 13A). At the end of the batches, the onset potential increased by ca. 0.10 V in both reactors (Figure 13B). The pH was near 6.7 during the CVs before the batches, but after the batches, the pH values were 6.87 and 6.95 in the abioFluBR and the abioFixBR, respectively.
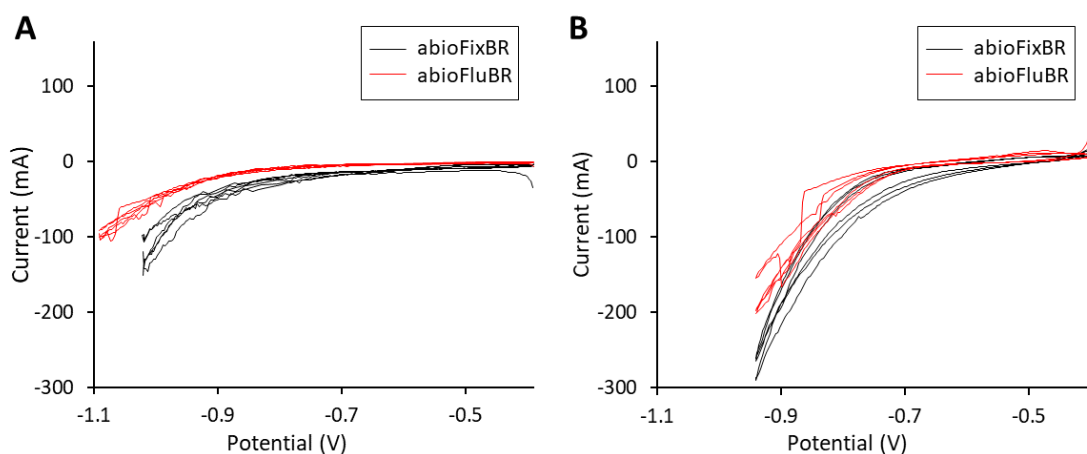
Figure 13. *The cyclic voltammogram of the abiotic fixed bed reactor (abioFixBR) (black) and the abiotic fluidized bed reactor (abioFluBR) (red) at (A) the beginning and at (B) the end of the 6- and 7-day experiments, respectively.*

3.1.2 Cathode potential and pH

To provide reducing equivalents at the cathode, the current was fixed to –70 mA in both abiotic reactors resulting in a current density of –6.0 A/m^2. The potential in response to the applied current was recorded during the batches (Figure 14). Despite some disturbances in the measured potential caused by CO_2 sparging and sampling for the pH (Figure 14A, red triangles) and the VFA measurements, the potential remained relatively

stable in the abioFluBR while the potential measured in the abioFixBR was noisier (Figure 14B). The average potential throughout the run in the abioFixBR was -0.90 ± 0.05 V, which is close to the abioFluBR (-0.92 ± 0.05 V).
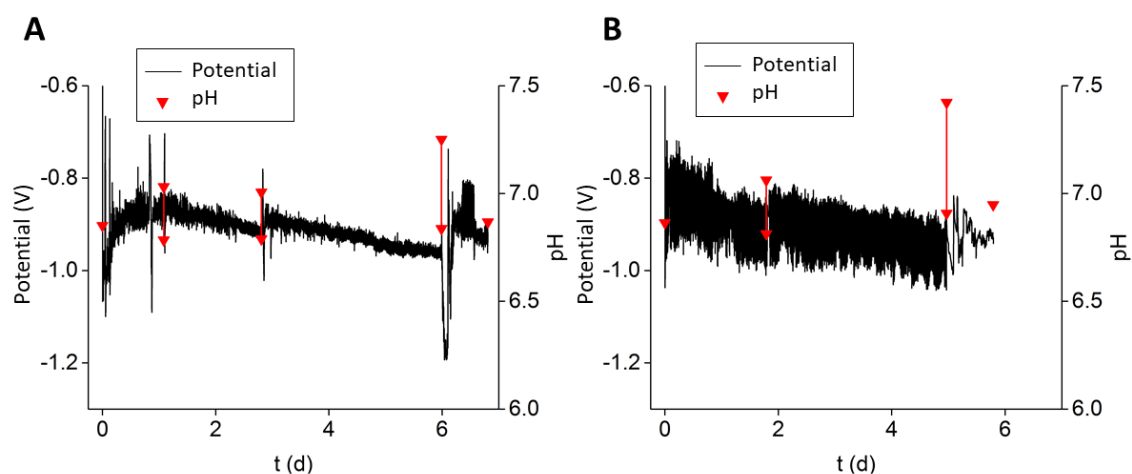
Figure 14. *The potential in V vs SHE (black) and the pH (red triangle) in (A) the abiotic fluidized bed reactor (abioFluBR) and (B) the abiotic fixed bed reactor (abioFixBR). The upper triangle is pH measured before sparging CO_2 and the lower is after the sparging.*

The pH values were relatively similar between the abioFluBR and the abioFixBR (Figure 14). The pH before the addition of CO_2 was on average 7.04 ± 0.16 in the abioFluBR and 7.14 ± 0.25 in the abioFixBR, but addition of CO_2 decreased the pH to 6.82 ± 0.04 and 6.86 ± 0.05 in the abioFluBR and the abioFixBR, respectively.

3.2 Biotic reactors

3.2.1 Current density

Electrons were provided to the microbes via the cathode by applying a current of -70 mA except for the first 7 days of chronoamperometry in the bioFixBR when the potential was fixed. The current density was -6.0 A/m^2 when the current was fixed to -70 mA. During the 7-day period of chronoamperometry in the bioFixBR, the pH decreased and the current became more negative right after CO_2 was added (Figure 15). Between the supplements, the pH increased and the current density became more positive (Figure 15).
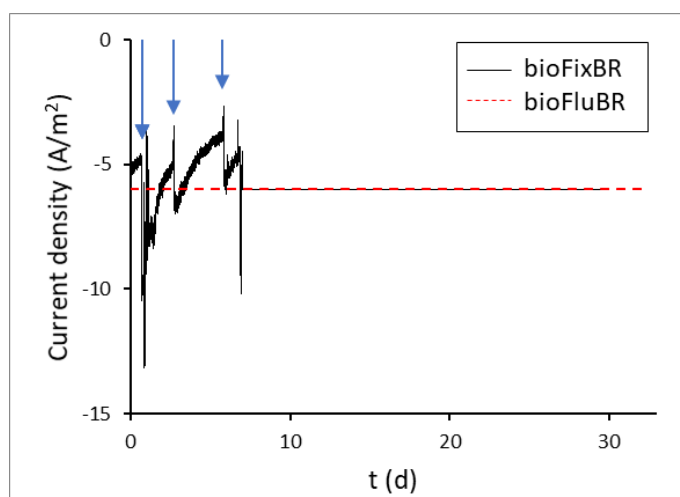
Figure 15. The current density normalized to the area of the membrane in the biotic fixed bed reactor (bioFixBR) (black solid line) and the biotic fluidized bed reactor (bioFluBR) (red dashed line). The blue arrows show the sampling and CO2 feeding during the chronoamperometric operation of the bioFixBR.

3.2.2 Cathode potential and pH

During the chronopotentiometric mode, the potentials were recorded (Figure 16). The initial potential was low (-1.12 ± 0.09 V) in the bioFluBR, but soon after changing the broken pump head (5 h after inoculation), it increased near -0.90 V and remained stable for the rest of the run (-0.99 ± 0.03 V) (Figure 16A). The operation method of the bioFixBR was changed to the chronoamperometric mode 7 days after inoculation, and the resulting potential was -0.76 ± 0.01 V from the 7th to the 16th day, after which it started to become more negative reaching -0.95 ± 0.01 V on the 26th day (Figure 16B). Then the potential became more positive again, reaching -0.87 ± 0.02 V (average from the last six hours).
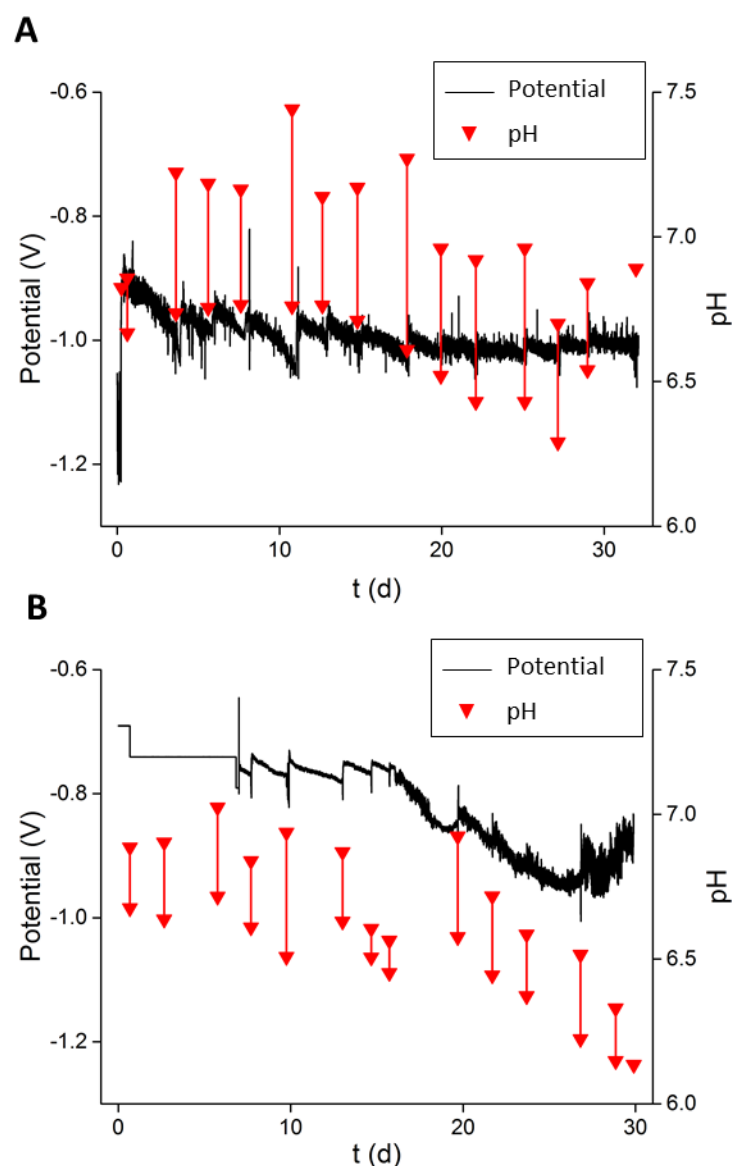
Figure 16. *The potential (black) and the pH (red) at the cathodes of the bioFluBR (A) and bioFixBR (B). In bioFixBR, the potential was fixed to –0.69 V, and then to –0.74 V, after which the current was fixed to –70 mA from the 7th day onwards.*

While the increased pH was accompanied by a more positive current in the chronoamperometric mode, the increased pH was inversely linked to a more negative potential during the chronopotentiometric mode (Figures 15 & 16). Before the CO_2 additions, the average pH from the 1st to the 13th day was 7.17 ± 0.19 in the bioFluBR and 6.91 ± 0.07 in the bioFixBR, but addition of CO_2 decreased the pH to 6.74 ± 0.04 and 6.63 ± 0.07 in the bioFluBR and the bioFixBR, respectively.

The pH values before the pH adjustments started to decrease in both reactors over time. In the bioFluBR, the initial pH values (pH before CO_2) decreased after the 20th day, but increased to 6.89 on the 32nd day (Figure 16A). The initial pH values of the bioFixBR started to decrease already after the 13th day, but on the 20th day (4 days since the previous

CO$_2$ addition) the pH had increased (Figure 16B). The pH values continued to decrease again after the 20th day reaching 6.14 on the 30th day.

3.2.3 Bacterial growth and acetate production

The OD$_{600nm}$ was measured to estimate the growth of suspended cells in the bioFluBR and the bioFixBR (Figure 17). The OD$_{600nm}$ of the bioFixBR increased from the initial OD$_{600nm}$ of 0.25 until it reached 1.23 on the 20th day, after which the growth of the suspended cells stagnated. Yet, the last measured OD$_{600nm}$ value leapt to 1.30. In the bioFluBR, the OD$_{600nm}$ increased slower as it increased from 0.23 to its highest value (1.0) 28 days after the inoculation. The OD$_{600nm}$ stayed around 1.0 until the 32nd day.
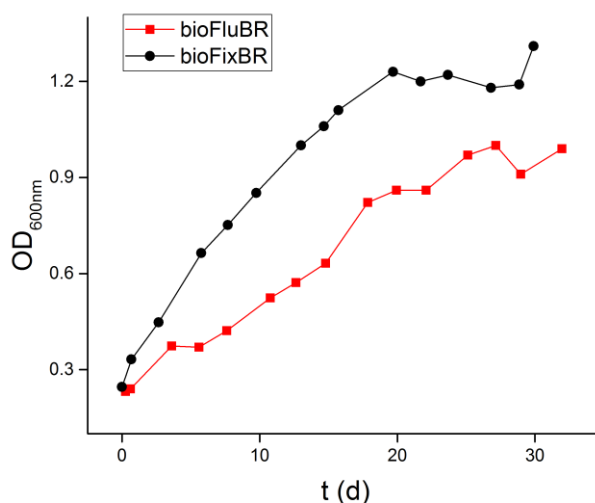
Figure 17. The development of optical density (OD$_{600nm}$) in the biotic fluidized bed reactor (bioFluBR) (red square) and the biotic fixed bed reactor (bioFixBR) (black circle).

The acetate concentration began to increase a day after inoculation in the bioFixBR, but a longer lag-phase was observed in the bioFluBR, where the acetate production started 6 days after inoculation (Figure 18). While the bioFluBR attained its final concentration of 5.14 g/L (87.11 mM) of acetate 32 days after inoculation, the final concentration in the bioFixBR reached 6.17 g/L (104.53 mM) 30 days after inoculation. The acetate concentration in the anode chamber of the bioFluBR was not measured, but approximately 2.60 g/L (44.25 mM) was measured from the anode chamber of the bioFixBR on the 30th day.
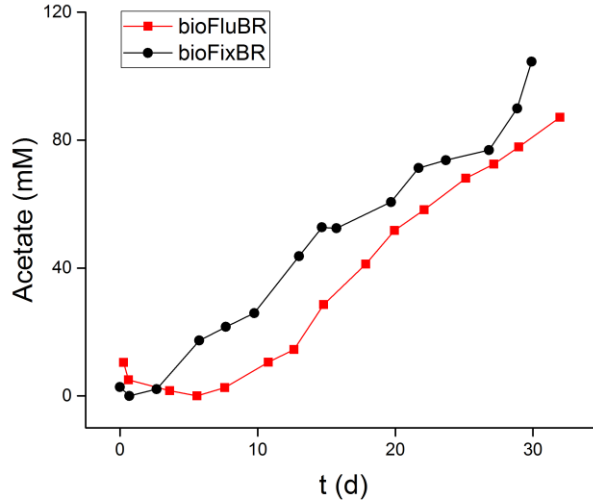
***Figure 18.** The change in the acetate concentration in the biotic fluidized bed reactor (bioFluBR) (red square) and the biotic fixed bed reactor (bioFixBR) (black circle).*

If the lag-phase is considered, the bioFluBR obtained its final titer (5.14 g/L) 26 days after the acetate production started (from the 6th to the 32nd day after inoculation). The bioFixBR had obtained similar concentration (5.31 g/L) 28 days after it started to produce acetate (from the 1st day to the 29th day).

Two weeks after the acetate production had started, the bioFluBR and the bioFixBR had reached their maximum acetate production rates and the CE on the 20th and the 15th day, respectively. The maximum and total volumetric productivities were similar between the bioFluBR and the bioFixBR (Table 4).

***Table 4.** The highest and the total volumetric productivities and the coulombic efficiencies from the biotic fluidized and fixed bed reactors.*

	Maximum			Total		
	Productivity (g/L/d)	CE[a] (%)	Days	Productivity (g/L/d)	CE[a] (%)	Days
bioFluBR[b]	0.21	37	6 - 20	0.20	34	6 - 32
bioFixBR[c]	0.22	40	1 - 15	0.21	37	1 - 30

[a]Abbreviation: CE, Coulombic efficiency. [b]Abbreviation: bioFluBR, biotic fluidized bed reactor. [c]Abbreviation: bioFixBR, biotic fixed bed reactor.

According to the chromatograms, butyrate started to appear in the bioFluBR and the bioFixBR. In the bioFixBR, butyrate was detected from the 15th day onwards reaching the highest titer of 0.59 g/L (6.80 mM) on the 30th day while the butyrate concentrations in the samples from the bioFluBR were below the lowest standard concentration thus not quantitated.

4 Discussion

The bioFixBR and the bioFluBR both produced acetate and even butyrate, but the abiotic controls did not. Therefore, biomass was required to catalyse the acetogenesis, which probably was H_2-mediated, because according to the CV analyses, H_2 was electrochemically produced at the selected current (–70 mA).

4.1 Acetate concentration and bacterial growth

As seen in Table 4, the bioFixBR and the bioFluBR reached similar total and maximum productivities and CEs. The maximum outputs were also achieved two weeks after the acetate production had started, even though the production had started later in the bioFluBR. Furthermore, the bioFixBR achieved a titer similar to the final titer of the bioFluBR in approximately the same time.

At the beginning, the acetate concentration (from the inocula) decreased in the bioFluBR and the bioFixBR although the concentration of the suspended cells (OD_{600nm}) increased from the 1st day. Residual O_2 could have been left in the cathode recirculation loop, from where it had possibly been removed by facultative anaerobic bacteria oxidizing acetate (Marshall *et al.* 2017), before the acetate concentration increased. The slower increase in the concentration of the suspended cells in the bioFluBR could explain the later increase in its acetate concentration. However, the relation of the biomass concentration to the OD_{600nm} was not determined and the biomass concentration at a certain OD_{600nm} may not be equal in the bioFluBR (GAC) and the bioFixBR (graphite granules). The OD_{600nm} measurements did not include the biomass immobilized as biofilm on the granules.

4.2 Comparing biotic reactors with literature

The granules increased the surface area of the cathode in the bioFixBR and the bioFluBR, but in the absence of a bed-free control (only the titanium mesh), the impact of just the granules on the performance is unknown. The maximum productivity and the maximum CE of the bioFixBR (0.22 g/L/d and 40 %) and the bioFluBR (0.21 g/L/d and 37 %) are similar to what Marshall *et al.* (2012) reported with 400 g/L of graphite granules and LaBelle *et al.* (2014) with a 10 cm^2 the graphite rod (Tables 1 & 4) in H-cell reactors. LaBelle *et al.* (2014) reported 14 ± 1 times higher productivity with 1000 g/L of graphite granules.

Because the graphite granule concentration used in the bioFixBR was approximately 70 g/L$_{catholyte}$ (280 g/L$_{cathode\ chamber}$), similar productivity was reached with less granules. Thus, the bioFixBR might have improved the production rate normalized to the cathode surface area, but the A$_{specific}$ of the graphite granules was unknown. Additionally, the concentration of GAC fluidized in the bioFluBR was 40 g/L$_{catholyte}$ (150 g/L$_{cathode\ chamber}$), which was significantly more than the 16 g/L of GAC Dong *et al.* (2018) fluidized with a magnetic stirrer. The bioFluBR also reached higher volumetric production (0.20 g/L/d), than what Dong *et al.* (2018) reported (0.14 g/L/d), although the difference is not as significant as in the GAC concentrations. On the other hand, normalizing the productivities to the surface area of a granular bed is not reasonable due to uncertainties e.g. in the charge distribution across a bed electrode (Quejigo *et al.* 2019). Moreover, the A$_{specific}$ varies between the granules.

4.3 Electrochemical behaviour

4.3.1 Cathode potential depended on pH

Supplementing CO_2 decreased the pH due to the formed carbonic acid, but between the supplements, the pH increased as the available protons were consumed into H_2 (Daniele *et al.* 1996; Marshall *et al.* 2013). During chronoamperometric mode, the reduced proton availability consequently would decrease the H_2 production rate and cause the more positive current as seen in Figure 15 (Jourdin *et al.* 2016; Marshall *et al.* 2013; Santos *et al.* 2018). However, when the current was fixed, the potential was observed to become more negative while the pH increased, which complies with Nernst equation (Equation 1). Over time, the pH became more acidic in the bioFluBR and more notably in the bioFluBR possibly due to the accumulation of produced organic acids (Patil *et al.* 2015). The pH may explain the changes in the potential in the abioFluBR, abioFixBR and the bioFluBR, but not entirely in the bioFixBR (Equation 1).

The potential was fixed to –0.74 V in the bioFixBR for the majority of the first 7 days, after which the current was fixed to –70 mA while the resulting potential remained almost the same (–0.76 ± 0.01 V). The pH could explain changes in the current and the potential until the 16th day, after which the potential started to become more negative despite the decreased pH. The lowest potential the bioFixBR reached was –0.95 ± 0.01 V while the potentials in the other reactors were on average –0.94 V throughout the runs. Starting the bioFixBR chronopotentiometrically would have been important for more reliable results

and to see, if the potential would have been closer to –0.94 V from the beginning. Additionally, analysing the gas composition could have provided information on the p_{H2}.

4.3.2 Onset potential shifted in abiotic tests

According to the voltammograms, the onset potential was ca. 0.1 V more negative in the abioFluBR than in the abioFixBR, which could have been caused by fluidization and/or the different bed materials. Furthermore, after the 7- and 6-day batches, the onset potentials were approximately 0.1 V more positive regardless of the higher pH. A decrease in p_{H2} could have caused the shift, but the gases were not analysed. Because biofilm could reduce the overpotential, the abiotic reactors could have been contaminated despite no VFAs were detected and potential CH_4 formation was inhibited by 2-bromoethanesulfonate. Another explanation could be a user error while performing the CVs. On the other hand, the metals in the medium might deposit on electrodes (Blanchet *et al.* 2015) and possible effects on the granules in the cathode chamber are unknown.

4.3.3 Does chronopotentiometric operation benefit MES?

Most of the MES studies referred to in here used chronoamperometry to produce acetate, but here the reactors were operated chronopotentiometrically. Because the onset potentials differed between the two reactor types, fixing the potential could have distorted the current density and possibly the acetate production.

Additionally, the chronopotentiometric mode possibly provided better tolerance against the changes in environmental factors compared to the chronoamperometric mode (Molenaar *et al.* 2017). During the 7-day period of the chronoamperometric operation of the bioFixBR, the onset potential for H_2 evolution at a higher pH or p_{H2} could have become more negative than the set potential (Equation 1). Because the electrochemical production rate of H_2 depends on the current density, chronopotentiometry could enable better control over the H_2 and thus the VFA production rates (Molenaar *et al.* 2017; Santos *et al.* 2018). However, not that many studies have reported using chronopotentiometric mode to produce acetate in MES.

4.4 Reactor optimization

Given that the reactors described here were the first iterations of such systems applied in MES, the bioFluBR and the bioFixBR reached relatively high acetate productivities (0.21 g/L and 0.22 g/L) and CEs (37 and 40 %). However, better results have been

reported in literature (Table 1 & 4), thus the reactor should be improved. Suggestions on improving the reactor configurations of this study, are discussed in the following chapters.

4.4.1 Reducing blockages and escape of granules from the reactor

Pausing the recirculation to sparge CO_2 into the recirculation bottle in this study hindered mixing inside the cathode chamber, which promoted the accumulation of H_2 in the cathode chamber (Kim and Kang 1997; Santos *et al.* 2018). Increasing the flow rate again after sparging improved the transfer of dissolved H_2 into the gas phase and the detachment of H_2 bubbles (Kim and Kang 1997; Santos *et al.* 2018), which were observed to carry GAC into the recirculation bottle. Installing the separate sparging port into the cathodic recirculation bottle of the bioFluBR probably prevented blockages by enabling the constant recirculation. Additionally, e.g. baffles could be installed inside the cathode chamber to help break bubbles and reduce the rate of escaping bed particles (Bello *et al.* 2017).

4.4.2 Reducing permeation of acetate through tubular CEM

Acetate was detected in the anode chamber of the bioFixBR indicating leakage or diffusion from the cathode chamber into the anode chamber. Due to the similar performance and configuration of the bioFluBR, acetate likely ended up in the anode chamber of the bioFluBR too. The seams of the tubular CEM could have leaked, which should be prevented by improving the preparation of the tubular CEM. However, in addition to cations, other species such as O_2, water, salts and possibly H_2 could permeate CEMs (Rozendal *et al.* 2006; Villaluenga *et al.* 2006).

The possible diffusion of VFAs through the CEM would probably have been driven by the greater hydrostatic pressure in the cathode chamber, caused by the higher flow rate and the height of the cathode chamber compared to the anode chamber (Trinke *et al.* 2016; Villaluenga *et al.* 2006). Increasing the anodic flow rate would decrease the pressure difference, but it could also help reduce the possible migration of O_2 into the cathode chamber at elevated current densities by decreasing the level of dissolved O_2 at the anode chamber (Kikuchi *et al.* 2009; Trinke *et al.* 2016; 2017). However, unwanted diffusion through the membrane could still occur to some extent.

4.4.3 Repositioning current collector to improve conductivity

The position of the current collector in the FluBRs and the FixBRs here was probably not the most optimum. Because the current collector was at the bottom of the reactor, the

maximum distance between a GAC particle and the collector was more than 8 cm (in the bioFluBR) and it would be even longer at a higher flow rate, which could negatively affect the distribution of electric charge (Hiddleston and Douglas 1970; Quejigo *et al.* 2019).

The configurations of FixBRs and FluBRs applied in MFC could be taken advantage to decrease the distance between the granules and the current collector in the reactors studied here. The current collector and the counter electrode could be pressed against the tubular membrane like Li *et al.* (2013) did (Figure 8B), although the consequently larger area of the current collector could increase the costs depending on the material (Krieg *et al.* 2018; Sharma *et al.* 2019). The size of a concentrically positioned current collector could be smaller while the distance between the collector, the granules and the counter electrode could be decreased by decreasing the ID of the cathode chamber. On the other hand, reducing the ratio of the ID to the static bed height (before fluidization) could increase the minimum velocity, and thus the energy required for fluidization (Bello *et al.* 2017).

4.4.4 Adjusting fluid flow rates to improve performance

The level of fluidization could be increased to improve the performance. Increasing the liquid flow would also increase the collisions of gas bubbles and the bed material, breaking the bubbles into smaller ones, which in turn increases the mass transfer between gas and liquid phases (Kim and Kang 1997). The consequent decrease in gas holdup could decrease the electric resistance of bubbles on the cathode surface and the probability of H_2 supersaturation (Castelló *et al.* 2020; Kim and Kang 1997; Santos *et al.* 2018).

On the other hand, increasing the flow rate could adversely reduce the collision rate between the particles, and thus the bed conductivity (Kim and Kang 1997; Quejigo *et al.* 2019). For instance, Kong *et al.* (2011) reported that increasing the superficial velocity of the liquid increased the generated current and power densities in FluBR-MFC up to 6.11 mm/s, after which the power density started to decrease. The flow rates together with the current densities should be optimized to provide enough CO_2, electrons and other substrates while still achieving proper mass transfer rates.

More research is needed as combining a three-phase biological FluBR, an electrochemical FluBR and MES makes the system relatively complex. Most importantly the control reactor (FixBR) should be as similar as possible with the FluBR. Another control such as a reactor without a carbon bed (with the titanium mesh) should be tested to understand the impact of just the current collector. For more comprehensive and reliable

understanding, more replicates should be conducted, and more variables should be tested. Due to the blockages for instance and leakages, the reactor was relatively challenging, which should be improved for industrial and cost-effective application of such a system.

5 Conclusions

The objective of this Master's thesis was to test the effect of the bioFluBR on bioelectrochemical production of acetate compared to the bioFixBR. It was demonstrated that both designed reactor types were successful in the production of acetate from CO_2 and electricity using a mixed microbiome. However, the FluBR was not confirmed to improve the performance, but more insight about the reactor design was achieved.

Minimizing the release of bubbles (mainly H_2) from the FluBR was important to improve the retention of the GAC-bed and to prevent blockages caused by recirculating GAC. This was achieved with a CO_2 sparging port in the recirculation bottle instead of the recirculation loop as the electrochemically produced H_2 was not able to accumulate during the 15 – 30 min sparging. However, when the bioFluBR was modified to help mitigate the issues, more differences were created between the bioFluBR and bioFixBR than just the bed material. Therefore, the FixBR is not a control for just the fluidization. For more reliable results, the flow rates should be the same between the reactors and they should be inoculated at the same time with an identical microbiome, in addition to minimizing other variation. Replicates should also be conducted.

However, the results between the bioFluBR (0.21 g/L/d and the 37 % CE) and the bioFixBR (0.22 g/L/d and 40 % CE) were similar despite the differences. The level of fluidization was 7 %, which was probably too small to cause significant difference between fluidized and fixed beds in terms of the mass transfers between the substrates, the biomass and the current collector. Better controls such as a bed-free reactor (with the titanium mesh) should be tested to understand how much the current collector alone affects the acetate production. If possible, the control bed material for the fluidization could be more similar to the GAC and more uniform than the graphite granules used here to make it easier to compare the performance.

More variables should be tested due to the complexity of the system. To enhance the acetate production, the liquid and gas flow rates as well as the current and the consequent production rate of H_2 needs to be adjusted to balance the mass transfer rate between the biomass, the bed particles, the current collector and the substrates. The flow rate at the anode chamber could be increased to reduce the hydrostatic pressure driven diffusion and loss of acetate from the cathode chamber to the anode chamber although the energy demand would increase.

On the other hand, the reactor needs to be optimized and simplified to enhance the production and to enable cost-effective, industrial application of such system. The difference of height between the anode and the cathode chambers should be reduced to decrease the losses caused by the pressure difference. Replacing the current collector at the bottom with a vertical current collector (a concentric rod or a tube along the membrane) would enable a higher bed with relatively low ohmic losses by decreasing the maximum distance between the bed particles and the collector. The preparation of the tubular membrane should also be changed to minimize leakages.

To replace fossil fuels with bioelectrochemically produced chemicals, further research is needed. The bioFixBR and bioFluBR have potential to advance MES, but further testing and optimizing is essential.

6 References

Bajracharya, S., Vanbroekhoven, K., Buisman, C. J. N., Pant, D. & Strik, D. P. B. T. B. (2016) Application of gas diffusion biocathode in microbial electrosynthesis from carbon dioxide. *Environ Sci Pollut Res* **23**: 22292–22308.

Batlle-Vilanova, P., Ganigué, R., Ramió-Pujol, S., Bañeras, L., Jiménez, G., Hidalgo, M., Balaguer, M. D., Colprim, J. & Puig, S. (2017) Microbial electrosynthesis of butyrate from carbon dioxide: Production and extraction. *Bioelectrochemistry* **117**: 57–64.

Bello, M. M., Abdul Raman, A. A. & Purushothaman, M. (2017) Applications of fluidized bed reactors in wastewater treatment – A review of the major design and operational parameters. *J Clean Prod* **141**: 1492–1514.

Blanchet, E., Duquenne, F., Rafrafi, Y., Etcheverry, L., Erable, B. & Bergel, A. (2015) Importance of the hydrogen route in up-scaling electrosynthesis for microbial CO_2 reduction. *Energy Environ Sci* **8**: 3731–3744.

Castelló, E., Nunes Ferraz-Junior, A. D., Andreani, C., Anzola-Rojas, M. del P., Borzacconi, L., Buitrón, G., Carrillo-Reyes, J., Gomes, S. D., Maintinguer, S. I., Moreno-Andrade, I., Palomo-Briones, R., Razo-Flores, E., Schiappacasse-Dasati, M., Tapia-Venegas, E., Valdez-Vázquez, I., Vesga-Baron, A., Zaiat, M. & Etchebehere, C. (2020) Stability problems in the hydrogen production by dark fermentation: Possible causes and solutions. *Renew Sustain Energy Rev* **119**: 109602.

Daniele, S., Lavagnini, I., Baldo, M.A. & Magno, F. (1996) Steady state voltammetry at microelectrodes for the hydrogen evolution from strong and weak acids under pseudo-first and second order kinetic conditions. *J Electroanal Chem* **404**: 105–111.

Deng, Q., Li, X., Zuo, J., Ling, A. & Logan, B. E. (2010) Power generation using an activated carbon fiber felt cathode in an upflow microbial fuel cell. *J Power Sources* **195**: 1130–1135.

Dong, Z., Wang, H., Tian, S., Yang, Y., Yuan, H., Huang, Q., Song, T. shun & Xie, J. (2018) Fluidized granular activated carbon electrode for efficient microbial electrosynthesis of acetate from carbon dioxide. *Bioresour Technol* **269**: 203–209.

Fargione, J., Hill, J., Tilman, D., Polansky, S. & Hawthorne, P. (2008) Land clearing and the biofuel carbon debt. *Science (80-)* **319**: 1235–1239.

Ganigué, R., Sánchez-Paredes, P., Bañeras, L. & Colprim, J. (2016) Low fermentation

pH is a trigger to alcohol production, but a killer to chain elongation. *Front Microbiol* **7**: 1–11.

Gao, Y., Liu, S., Cai, Q., Li, H. & Yang, P. (2019) Effects of chloride ion on performance and microbial community in an anaerobic fluidized bed microbial fuel cell. *Environ Eng Sci* **36**: 1214–1223.

Gildemyn, S., Verbeeck, K., Jansen, R. & Rabaey, K. (2017) The type of ion selective membrane determines stability and production levels of microbial electrosynthesis. *Bioresour Technol* **224**: 358–364.

Groh, E. D. & Möllendorff, C. v. (2020) What shapes the support of renewable energy expansion? Public attitudes between policy goals and risk, time, and social preferences. *Energy Policy* **137**: 111171.

Haavisto, J. M., Kokko, M. E., Lay, C. H. & Puhakka, J. A. (2017) Effect of hydraulic retention time on continuous electricity production from xylose in up-flow microbial fuel cell. *Int J Hydrogen Energy* **42**: 27494–27501.

He, Y., Liu, Z., Xing, X. hui, Li, B., Zhang, Y., Shen, R., Zhu, Z. & Duan, N. (2015) Carbon nanotubes simultaneously as the anode and microbial carrier for up-flow fixed-bed microbial fuel cell. *Biochem Eng J* **94**: 39–44.

Hiddleston, J. N. & Douglas, A. F. (1970) Current/potential relationships and potential distribution in fluidized bed electrodes. *Electrochim Acta* **15**: 431–443.

Huang, J., Yang, P., Guo, Y. & Zhang, K. (2011) Electricity generation during wastewater treatment: An approach using an AFB-MFC for alcohol distillery wastewater. *Desalination* **276**: 373–378.

Jourdin, L., Freguia, S., Flexer, V. & Keller, J. (2016) Bringing high-rate, CO_2-based microbial electrosynthesis closer to practical implementation through improved electrode design and operating conditions. *Environ Sci Technol* **50**: 1982–1989.

Jourdin, L., Raes, S. M. T., Buisman, C. J. N. & Strik, D. P. B. T. B. (2018) Critical biofilm growth throughout unmodified carbon felts allows continuous bioelectrochemical chain elongation from CO_2 up to caproate at high current density. *Front Energy Res* **6**: 1–15.

Khanal, S. (2008a) Biohydrogen production: Fundamentals, challenges, and operation strategies for enhanced yield. In: S. Khanal (ed.), Anaerobic biotechnology for bioenergy

production: Principles and applications, pp. 189–220. Blackwell Publishing, Singapore.

Khanal, S. (2008b) Microbiology and biochemistry of anaerobic biotechnology. In: Khanal S. (ed.), Anaerobic biotechnology for bioenergy production: Principles and applications, pp. 29–42. Blackwell Publishing, Singapore.

Kim, J. H. & Alameri, S. A. (2019) Harmonizing nuclear and renewable energy: Case studies. *Int J Energy Res* 1–9.

Kim, S. D. & Kang, Y. (1997) Heat and mass transfer in three-phase fluidized-bed reactors - an overview. *Chem Eng Sci* **52**: 3639–3660.

Kikuchi, K., Ioka, A., Oku, T., Tanaka, Y., Saihara, Y. & Ogumi, Z. (2009) Concentration determination of oxygen nanobubbles in electrolyzed water. *J colloid interface Sci* **329**: 306–309.

Kong, W., Guo, Q., Wang, X. & Yue, X. (2011) Electricity generation from wastewater using an anaerobic fluidized bed microbial fuel cell. *Ind Eng Chem Res* **50**: 12225–12232.

Kracke, F., Vassilev, I. & Krömer, J. O. (2015) Microbial electron transport and energy conservation – The foundation for optimizing bioelectrochemical systems. *Front Microbiol* **6**: 1–18.

Krieg, T., Madjarov, J., Rosa, L., Enzmann, F., Harnisch, F., Holtmann, D. & Rabaey, K. (2018) Reactors for microbial electrobiotechnology. *Adv Biochem Eng Biotechnol* **123**: 127–141.

Krieg, T., Sydow, A., Schröder, U., Schrader, J. & Holtmann, D. (2014) Reactor concepts for bioelectrochemical syntheses and energy conversion. *Trends Biotechnol* **32**: 645–655.

LaBelle, E. V., Marshall, C. W., Gilbert, J. A. & May, H. D. (2014) Influence of acidic ph on hydrogen and acetate production by an electrosynthetic microbiome. *PLoS One* **9**: e109935.

LaBelle, E. V. & May, H. D. (2017) Energy efficiency and productivity enhancement of microbial electrosynthesis of acetate. *Front Microbiol* **8**: 756.

Levi, P. G. & Cullen, J. M. (2018) Mapping global flows of chemicals: from fossil fuel feedstocks to chemical products. *Environ Sci Technol* **52**: 1725–1734.

Li, W., Jiang, N., Hu, B., Liu, X., Song, F., Han, G., Jordan, T. J., Hanson, T. B., Liu, T. L. & Sun, Y. (2018) Electrolyzer design for flexible decoupled water splitting and organic

upgrading with electron reservoirs. *Chem* **4**: 637–649.

Li, X., Zhu, N., Wang, Y., Li, P., Wu, P. & Wu, J. (2013) Animal carcass wastewater treatment and bioelectricity generation in up-flow tubular microbial fuel cells: Effects of HRT and non-precious metallic catalyst. *Bioresour Technol* **128**: 454–460.

Logan, B. E., Hamelers, B., Rozendal, R., Schröder, U., Keller, J., Freguia, S., Aelterman, P., Verstraete, W. & Rabaey, K. (2006) Microbial fuel cells: Methodology and technology. *Environ Sci Technol* **40**: 5181–5192.

Logan, B. E., Rossi, R., Ragab, A. & Saikaly, P. E. (2019) Electroactive microorganisms in bioelectrochemical systems. *Nat Rev Microbiol* **17**: 307–319.

Maric, R. & Yu, H. (2019) Proton exchange membrane water electrolysis as a promising technology for hydrogen production and energy storage. In: Fedorenko Y. (ed.), Nanostructures in energy generation, transmission and storage, pp. 95–117. IntechOpen.

Marshall, C. W., Ross, D. E., Fichot, E. B., Norman, R. S. & May, H. D. (2012) Electrosynthesis of commodity chemicals by an autotrophic microbial community. *Appl Environ Microbiol* **78**: 8412–8420.

Marshall, C. W., Ross, D. E., Fichot, E. B., Norman, R. S. & May, H. D. (2013) Long-term operation of microbial electrosynthesis systems improves acetate production by autotrophic microbiomes. *Environ Sci Technol* **47**: 6023–6029.

Marshall, C. W., Ross, D. E., Handley, K. M., Weisenhorn, P. B., Edirisinghe, J. N., Henry, C. S., Gilbert, J. A., May, H. D. & Norman, R. S. (2017) Metabolic reconstruction and modeling microbial electrosynthesis. *Sci Rep* **7**: 1–12.

Molenaar, S. D., Saha, P., Mol, A. R., Sleutels, T. H. J. A., ter Heijne, A. & Buisman, C. J. N. (2017) Competition between methanogens and acetogens in biocathodes: A comparison between potentiostatic and galvanostatic control. *Int J Mol Sci* **18**: 204.

Nevin, K. P., Woodard, T. L., Franks, A. E., Summers, Z. M. & Lovley, D. R. (2010) Microbial electrosynthesis: Feeding microbes electricity to convert carbon dioxide and water to multicarbon extracellular organic compounds. **1**: 1–4.

Pandey, D. (2002) Global climate change and carbon management in multifunctional forests. *Curr Sci* **83**: 593–602.

Patil, S. A., Arends, J. B. A., Vanwonterghem, I., Van Meerbergen, J., Guo, K., Tyson,

G. W. & Rabaey, K. (2015) Selective enrichment establishes a stable performing community for microbial electrosynthesis of acetate from CO_2. *Environ Sci Technol* **49**: 8833–8843.

Paul, R., Zemlyanov, D., Roy, A. K. & Voevodin, A. A. (2019) Characterization techniques and analytical methods of carbon-based materials for energy applications. In: Paul, R., Etacheri, V., Wang, Y. & Lin, C.-T. (eds.), Carbon based nanomaterials for advanced thermal and electrochemical energy storage and conversion, pp. 63–88. Elsevier Inc, Amsterdam.

Potter, M. C. (1911) Electrical effects accompanying the decomposition of organic compounds. *Proc R Soc B Biol Sci* **84**: 260–276.

Quejigo, J. R., Tejedor-Sanz, S., Esteve-Núñez, A. & Harnisch, F. (2019) Bed electrodes in microbial electrochemistry: setup, operation and characterization. *ChemTexts* **5**: 1–15.

Rabaey, K., Clauwaert, P., Aelterman, P. & Verstraete, W. (2005) Tubular microbial fuel cells for efficient electricity generation. *Environ Sci Technol* **39**: 8077–8082.

Rabaey, K. & Rozendal, R. A. (2010) Microbial electrosynthesis - Revisiting the electrical route for microbial production. *Nat Rev Microbiol* **8**: 706–716.

Rozendal, R. A., Hamelers, H. V. M., Euverink, G. J. W., Metz, S. J. & Buisman, C. J. N. (2006) Principle and perspectives of hydrogen production through biocatalyzed electrolysis. *Int J Hydrogen Energy* **31**: 1632–1640.

Saady, N. (2013) Homoacetogenesis during hydrogen production by mixed cultures in dark fermentation: Unresolved challenge. *Int J Hydrogen Energy* **38**: 13172–13191.

Santos, D. M. F., Sequeira, C. & Figueiredo, J. (2018) Hydrogen production by alkaline water electrolysis. *Quim Nova* **36**: 1176–1193.

Sharma, K. R. (2008) Kinetics and modeling in anaerobic processes. In: Khanal S. (ed.), Anaerobic biotechnology for bioenergy production: Principles and applications, pp. 65–92. Blackwell Publishing, Singapore.

Sharma, M., Alvarez-Gallego, Y., Achouak, W., Pant, D., Sarma, P. M. & Dominguez-Benetton, X. (2019) Electrode material properties for designing effective microbial electrosynthesis systems. *J Mater Chem A* **7**: 24420–24436.

Siegert, M. (2018) A scalable multi-channel software potentiostat. *Front Energy Res* **6**:

1–4.

Tremblay, P. L., Faraghiparapari, N. & Zhang, T. (2019) Accelerated H_2 evolution during microbial electrosynthesis with *Sporomusa ovata*. *Catalysts* **9**: 1–11.

Trinke, P., Bensmann, B. & Hanke-Rauschenbach, R. (2017) Current density effect on hydrogen permeation in PEM water electrolyzers. *Int J Hydrogen Energy* **42**: 14355–14366.

Trinke, P., Bensmann, B., Reichstein, S., Hanke-Rauschenbach, R. & Sundmacher, K. (2016) Hydrogen permeation in PEM electrolyzer cells operated at asymmetric pressure conditions. *J Electrochem Soc* **163**: F3164–F3170.

Vassilev, I., Hernandez, P. A., Batlle-Vilanova, P., Freguia, S., Krömer, J. O., Keller, J., Ledezma, P. & Virdis, B. (2018) Microbial electrosynthesis of isobutyric, butyric, caproic acids, and corresponding alcohols from carbon dioxide. *ACS Sustain Chem Eng* **6**: 8485–8493.

Vassilev, I. (2019) Microbial electrosynthesis: Anode- and cathode-driven bioproduction of chemicals and biofuels. University of Queensland. Doctoral dissertation.

Vassilev, I., Kracke, F., Freguia, S., Keller, J., Krömer, J. O., Ledezma, P. & Virdis, B. (2019) Microbial electrosynthesis system with dual biocathode arrangement for simultaneous acetogenesis, solventogenesis and carbon chain elongation. *Chem Commun* **55**: 4351–4354.

Villaluenga, J. P. G., Barragán, V. M., Seoane, B. & Ruiz-Bauzá, C. (2006) Sorption and permeation of solutions of chloride salts, water and methanol in a Nafion membrane. *Electrochim Acta* **51**: 6297–6303.

Vincent, K.A., Parkin, A. & Armstrong, F.A. (2007) Investigating and exploiting the electrocatalytic properties of hydrogenases. *Chem Rev* **107**: 4366–4413.

Worstell, J. (2014) Adiabatic fixed-bed reactors: Practical guides in chemical engineering, pp. 13–33. Butterworth-Heinemann, Kidlington.

Wrigley, E. A. (2013) Energy and the english industrial revolution. *Philos Trans R Soc A Math Phys Eng Sci* **371**: 20110568.

Zhang, Y. & Angelidaki, I. (2014) Microbial electrolysis cells turning to be versatile technology: Recent advances and future challenges. *Water Res* **56**: 11–25.